Multi-timescale neural adaptation underlying long-term musculoskeletal reorganization.

*Roland Philipp[1,2], Yuki Hara[3], Naoki Uchida[1,2], Naohito Ohta[1,2], Tomomichi Oya[1,4], Tetsuro Funato[2], and *Kazuhiko Seki[1]

[1]National Center of Neurology and Psychiatry, Department of Neurophysiology, 4-1-1 Ogawa-Higashi, Kodaira, Tokyo 1878502, Japan
[2]University of ElectroCommunications, Graduate School of Informatics and Engineering, Dept. of Mechanical and Intelligent Systems Engineering. W2-217, 1-5-1 Chofugaoka, Chofu, Tokyo, Japan
[3]National Center of Neurology and Psychiatry, Department of Orthopaedic Surgery, 4-1-1 Ogawa-Higashi, Kodaira, Tokyo 1878502, Japan
[4]Western Institute for Neuroscience, University of Western Ontario, London, N6A 3K7, Canada

*Corresponding authors:
Kazuhiko Seki and Roland Philipp
Email: seki@ncnp.go.jp and roland@ncnp.go.jp

Author Contributions: R.P. and K.S. designed all experiments and wrote the paper. R.P., Y.H., N.U., and N.O. performed the experiments and analyzed the data. R.P., Y.H., T.O., and K.S. performed the surgeries. T.F. provided conceptual advice and wrote the paper. All authors reviewed the results and approved the final version of the manuscript.

Competing Interest Statement: The authors declare no competing interests.
Classification: Biological Sciences. Neuroscience
Keywords: tendon transfer, muscle synergy, electromyography, non-human primate

This PDF file includes:
Main Text
Figures 1 to 7

ABSTRACT

The central nervous system (CNS) can effectively control body movements despite environmental changes. While much is known about adaptation to external environmental changes, less is known about responses to internal bodily changes. This study investigates how the CNS adapts to long-term alterations in the musculoskeletal system using a tendon transfer model in non-human primates. We surgically relocated finger flexor and extensor muscles to examine how the CNS adapts its strategy for finger movement control by measuring muscle activities during grasping tasks. Two months post-surgery, the monkeys demonstrated significant recovery of grasping function despite the initial disruption. Our findings suggest a two-phase CNS adaptation process: an initial phase enabling function with the transferred muscles, followed by a later phase abolishing this enabled function and restoring a more efficient and “good enough” control strategy resembling the original. These results highlight a multi-phase CNS adaptation process with distinct time constants in response to sudden bodily changes, offering potential insights into understanding and treating movement disorders.

SIGNIFICANCE STATEMENT

This study demonstrates the remarkable ability of the CNS to adapt motor control to long-term internal changes, even after significant alterations to the musculoskeletal system. These findings expand our understanding of CNS plasticity and offer promising insights for enhancing rehabilitation following injuries or surgeries that disrupt body mechanics. By unraveling the mechanisms behind this long-term adaptation, targeted rehabilitation strategies to optimize motor recovery in patients with stroke, spinal cord injury, or musculoskeletal disorders can be developed, ultimately improving patient outcomes and quality of life.

INTRODUCTION:

The central nervous system (CNS) fundamentally adapts bodily functions in response to various environmental changes. These environmental changes can be external (such as altered gravity conditions experienced during space travel) or internal (like gradual changes in an animal's body size and shape throughout its lifespan) [1]. Previous research has primarily addressed the external changes by developing unique experimental approaches to understand CNS adaptation. For example, the prism adaptation paradigm [2, 3] requires subjects to wear glasses with prisms that shift or reverse the visual field, necessitating the subject's motor system to adapt to the altered visual world for accurate reaching movements [4]. Similarly, the force-field adaptation paradigm [5, 6] introduces a bias to proprioceptive feedback for a given movement, compelling subjects to adjust their motor system to the manipulated external proprioceptive world. These experimental settings have served as excellent models for understanding how motor function adapts to changes in the external environment.

In contrast, CNS adaptations to internal changes within the body are less understood. Adaptative mechanisms to rapid and transient bodily changes, such as muscle fatigue [7], postural sway [8] or disorientation from swift bodily rotations [9], have been established. However, the CNS response to prolonged internal bodily changes is less explored, primarily due to limited availability of experimental approaches for modeling long-term bodily changes. Therefore, the mechanisms by which the CNS adjusts its motor control strategy to accommodate long-term changes in the musculoskeletal system, allowing consistent movements despite varying internal body features, are unclear. This lack of knowledge hinders our understanding of the pathophysiological mechanisms of chronic human diseases, where long-term, maladaptive changes in the musculoskeletal system are often observed [10].

Here, we present an experimental approach involving tendon transfer (TT) surgery to explore how animals adjust limb control when their musculoskeletal system undergoes long-term changes. The TT model offers a unique perspective on CNS plasticity in response to changes in the internal physical environment [11]. This model contrasts with those involving CNS lesions, where the CNS injury itself triggers complex and less predictable CNS plasticity, potentially skewing assessment of its adaptive capabilities. Tendon transfer is a well-established surgical procedure used in rodent and feline models and human patients.

Previous studies suggest that adult rodents are less adaptable to changes in the musculoskeletal system compared with younger rodents and other species [11, 12]. While young rodents may exhibit some recovery and compensation following TT, the underlying plasticity processes may differ from those in adults [13, 14]. Alternatively, cats show motor coordination adjustments after forelimb muscle cross-transfers [15, 16]. In humans, cortical plasticity has been observed following surgical TT [17-19]. Collectively, these findings highlight a gradient of adaptability, with rodents demonstrating minimal or no adaptation, cats exhibiting partial adaptation, and primates (including humans) demonstrating full adaptation to musculoskeletal changes. Therefore, adaptability to TT is a feature of a highly evolved CNS in non-human primates and humans. However, the exact organization and temporal progression of these CNS adaptations post-TT surgery remains to be elucidated.

This study aimed to identify long-term adaptive mechanisms of the CNS to managing changes in the musculoskeletal system, specifically in non-human primates. We surgically altered the musculoskeletal system by cross-union of the finger extensor and flexor muscle tendons. Our focus was to determine how these modifications impact CNS regulation of limb muscle activity during recovery. The primary metric for this adaptation was change in finger-grasping task control. Through this analysis, we sought to better understand long-term adaptations of the CNS to substantial changes in the body's musculoskeletal configuration.

RESULTS

In this study, we developed a novel tendon cross-union animal model. This involved surgically swapping the tendons of two antagonistic finger muscles in a macaque monkeys' forearm (Fig. 1). The effectiveness and consistency of the surgery was confirmed by measuring: (i) the distance traveled by muscle fibers and their intramuscular tendons in the transferred muscle (Fig. 1C, D); and (ii) the amount of fingertip displacement (Fig. 1E, F). Both measurements were induced by percutaneous electrical stimulation over the transferred muscles (Fig. 1B). For a detailed description of the results of these measurements see the Methods section. Here, we will primarily discuss the adaptations observed by electromyography (EMG) post-tendon transfer (TT), as well as behavioral recovery in the monkey. The two monkeys were assigned slightly different tasks, allowing us to examine controlled grasping in Monkey A and a more natural grasp in Monkey B (refer to the Methods section, and Figs. 2 and S1 for further details). Once the monkeys had mastered their respective tasks, we recorded control sessions and then performed the tendon cross-union. Post-surgery, and once the monkeys had fully recovered and were able to perform the task independently (~3–4 weeks), EMG recordings and behavior were examined. Despite the now reversed roles of the transferred muscles, the monkeys were able to recover their grasping performance within two months (Fig. S2). However, none of the parameters measured returned promptly to pre-TT levels. For example, contact time with the object (in Monkey A) or food (in Monkey B) were much longer immediately after TT than in the first 6 (or 5) sessions post-TT (197.7 ± 92.2 vs. 660.6 ± 221 ms and 169.7 ± 14 vs. 316.3 ± 31.9 ms, respectively; $p < 0.05$, two-sample *t*-test; filled squares in Fig. S2). It took around 10 days for both monkeys to recover back to pre-TT levels ($p > 0.05$, two-sample *t*-test) and fully stabilize (after 20 and 32 days, respectively). All measured indices eventually returned to pre-TT levels by the end of the experiment.

Transferred muscles exhibited antagonistic EMG activity post-TT

Initially, we investigated whether EMG activity exhibited any changes post-TT. Given that we interchanged the tendons of an antagonistic muscle pair (specifically the finger flexor and extensor), a biomechanically sound adaptation would be to use the former finger extensor (extensor digitorum communis, EDC)

for finger flexion, and the finger flexor (flexor digitorum superficialis, FDS) for finger extension during a grasping task. Our focus was to determine if these expected changes did indeed occur by EMG of both the transferred and non-transferred muscles.

Figure 3 shows a comparison of EMG activity profiles for the two transferred muscles, EDC and FDS, in Monkey A (Fig. 3A–D). Prior to surgery, the control showed distinct and contrasting EMG profiles in both muscles. For instance, peak activity in EDC (▼) occurred long after completion of the grasping action (indicated by vertical dashed lines at 0% task range) at 15% task time (Fig. 3A), coinciding with the animal pre-shaping its hand to prepare for the subsequent grasp. Whereas peak activity in FDS (▽) was observed immediately after completion of the grasping action (0.49%; Fig. 3C). The question we posed was whether the post-surgery activity of EDC resembled its original profile (without adaptation to surgery) or the activity of FDS (the anticipated profile following surgical adaptation), and vice versa. Our findings suggested that EMG activity was altered to assume a new function, as anticipated from the transferred muscle. Early after TT, peak activity of EDC occurred at -0.58% task time (Fig. 3B; days 29 [red line] and 64 [orange]), which aligns with peak activity of FDS prior to TT (Fig. 3C; black line). Also, for FDS, peak activity occurred at 11% task time (Fig. 3D; ▼), which aligned with peak activity of EDC (Fig. 3A).

This was corroborated by the results in Monkey B (Fig. S3). Although the EMG patterns of both muscles varied significantly as the two monkeys performed different types of grasping actions, we found that the EMG of EDC peaked at -6.12% before (Fig. S3A; ▼) and 0.35% and 1.05% after TT (Fig. S3B; ▽, days 22 and 36, respectively), closely matching the timing for FDS control data (Fig. S3C). Note that the corresponding analysis using FDS could not be performed in Monkey B, since the EMG signal of FDS was lost early after TT (see Methods for details).

We were able to extend our recordings to 122- and 64-days post-TT for monkeys A and B, respectively. This allowed us to examine whether the adaptations observed in the early period were consistent throughout the experimental period. These additional days (Fig. 3B, D; 69 [cyan], 79 [blue], and 99 [black] post-TT; see Fig. S6 for recordings from all days) showed that the EMG activity profiles for both muscles unexpectedly returned to their pre-surgery state. For example, as already described, the EMG signal of EDC at days 29 and 64 shared the characteristics of FDS, but by the following day (only 5 days later, day 69 [light

blue] post-TT) already exhibited pre-TT characteristics of EDC, continuing as such until the end of the recording period (day 79 [blue] and 99 [black]). This was confirmed for the EDC muscle of Monkey B (Fig. S3A, B; Fig. S7 for recordings from all days).

Figure 3E illustrates cross-correlation coefficients between the EDC EMG profile post-TT (EDC-post) and the original EDC control data (EDC-pre) in Monkey A. Figure 3G shows coefficients for EDC-post and FDS-pre correlations in the same monkey. The coefficient corresponding to the original profile decreased to between -0.3 and 0.2 over approximately 65 days (Fig. 3E). In contrast, the coefficient corresponding to the expected EMG profile exhibited an inverse pattern, with low coefficients pre-TT and a high coefficient (of 0.9) post-TT (Fig. 3F). Cross-correlation analysis for FDS (Fig. 3F–H) revealed a similar pattern. Cross-correlation coefficients for FDS-pre- vs. FDS-post-analysis declined from 1 to negative values, only to rebound to their original values within a month (day 79; Fig. 3F). This outcome aligns with our previous observations (Fig. 3B, D), and were corroborated by the results from Monkey B (Fig. S3). Here, cross-correlation coefficients dropped from +0.95 to +0.1 for EDC-pre vs. EDC-post comparison, and increased from -0.5 to 0.9 for the FDS-pre- vs. FDS-post comparison (Fig. S3D, E). After 42 days post-TT, cross-correlation coefficients started to gradually increase or decrease to +0.9 and -0.7, respectively. This indicates that the anticipated initial changes in EMG activity profiles are not permanent. Instead, they revert to their original patterns two months post-TT.

In summary, both monkeys exhibited a two-phase adaptation following TT: an early and a late phase. Early adaptation endowed the transferred muscles with new functionality, as predicted. Late adaptation reinstated the pre-TT EMG profile.

Non-transferred muscles exhibited characteristic changes in EMG activity post-TT

Interestingly, changes in EMG pattern were not isolated to the transferred muscles. When the analysis was repeated on non-transferred muscles in both monkeys (Figs. S4–9), we also found comparable changes in some muscles. This quantitative analysis is described in the next section; here, we briefly describe activity characteristics. In Monkey A, similar changes as in the EDC (Fig. 3A, B) were also found in extensor digitorum-2,3 (ED23), extensor carpi ulnaris (ECU), and extensor carpi radialis (ECR) (Fig. S4B–D and L–N), i.e., an initial shift of activity towards FDS that was followed by a later reversion to the original pattern.

Similarly, changes in flexor carpi ulnaris (FCU) (Fig. S4G, Q) mimicked that observed in FDS (Fig. 3C, D). We found that the non-transferred muscles in Monkey B (Fig. S5) also exhibited the changes observed in the transferred muscles. For example, ED23, ED45, ECU, and flexor digitorum profundus (FDP) (e.g., ED23; Fig. S5N) exhibited similar changes as in EDC (Fig. S5M), initially adopting flexor properties and later reverting to their original pattern.

In addition, some muscles also exhibited a patten that was incompatible with the transferred muscles. For example, before TT, PL, and flexor carpi radialis (FCR) exhibited peak activity at event alignment (e.g., PL at object release; Fig. S4H), which again increased gradually over time towards the end of the shown task range. After TT, however, the amplitude of both peaks initially decreased drastically, followed by a consistent increase in the amplitude of the later peak. There was no two-step change observed in the transferred muscles in any of the subsequent recording days (Fig. S4R).

Muscle synergies exhibited antagonistic properties post-TT

Alternation of EMG activity in non-transferred muscle suggests an interesting possibility: TT might alter the control strategy of coordinated muscle activity for hand movement by modifying the transferred muscles and their agonists as a cohesive unit (i.e., muscle synergy). To test this, we conducted a similar analysis on temporal activation coefficients of muscle synergies. We computed synergy weights (Fig. 4B–E for Monkey A; and Fig. S10 for Monkey B) and temporal activation coefficients (Fig. 4F–I for Monkey A; and Fig. S10F–I for Monkey B) from EMGs using non-negative matrix factorization (NMF) [20]. We extracted four muscle synergies that accounted for more than 80% [21] of the ‘variance accounted for’ (VAF) (Figs. 4A and S10A, 85% for both monkeys; the results of the original and shuffled data sets are shown). Among these synergies, one was a finger flexor synergy and another was a finger extensor synergy, identified before the tendon cross-transfer in each monkey (Fig. 4B, C). These were referred to as synergy A and synergy B, respectively.

We examined if the composition and activation coefficient of each synergy changed, corresponding to the changes observed in the transferred and non-transferred muscles. First, we analyzed changes in the composition of these synergies. The cosine distance for the same synergy pairs (e.g., synergy A of pre-TT and synergy A of post-TT) was low (mean [± SD]: 0.03 [± 0.03] in Monkey A and 0.09 [± 0.11] in Monkey B) and different pairs (e.g., synergy A of pre-TT

and synergy B of post-TT) was high (mean [± SD]: 0.67 [± 0.08] in Monkey A and 0.61 [± 0.14] in Monkey B). There was a one-to-one correspondence between synergy pairs ($p < 0.01$, two-way analysis of variance [ANOVA] due to synergy factor; $p < 0.01$, Bonferroni post-hoc test between synergy of the same pair and different pair). This was demonstrated in both monkeys (Figs. 4B–E, S10B–E). These results indicate that the composition of these four synergies and the contribution of each muscle do not change drastically before and after TT surgery. Figure 4F–I presents a comparison of the activation coefficients for all four muscle synergies, before and after the TT procedure (for Monkey B, refer to Fig. S10F–I; Fig. S11 for all experimental days). Prior to TT, the activation coefficients for the flexor synergy (synergy A) reached a peak at +0.97% (Fig. 4F). Post-TT, these coefficients shifted towards later times shortly after surgery (+10.7%), but eventually returned to their original timing. Meanwhile, the extensor synergy (synergy B) peaked at 12.62% pre-TT and moved to -0.97% shortly after surgery. Like the flexor synergy, the extensor synergy also reverted to its original timing in subsequent sessions (Fig. 4G). These characteristics corresponded well to the ones found in the transferred muscles (Fig. 3), supporting our hypothesis that the transferred muscle and its agonist changes as a cohesive unit.

Figure 4H shows the temporal changes for synergy C, a wrist flexor synergy (Fig. 4D). While two peaks were observed prior to surgery (+1.46% and +15%), the early post-surgery sessions did not exhibit any significant peaks. However, later sessions displayed a single peak at +14.59% task time, with an increasing magnitude as a function of recovery days. These characteristic changes corresponded well to a patten that was incompatible to the transferred muscles found in FCR and PL, as described above. Indeed, both muscles showed highest synergy weights for this synergy (Fig. 4D). Synergy D was a wrist extensor synergy (Fig. 4E), and underwent a single notable change on day 29, but quickly reverted to its original pattern (Fig. 4I). These pattens of changes in synergy 3 and 4, both contributed minimally to the EMG of transferred muscles. This suggests that some non-transferred muscles change their EMG activity following the mode, which is independent to the one observed in the transferred muscle and may reinforce the functional adaptation made by the transferred muscle and its synergists.

Several of these results were also confirmed in Monkey B. Activation coefficients of extensor synergy B peaked at -8.75% before TT, increasing to +3.5% after TT (Fig. S10G). This peak activity persisted until the last day (day 69 post-TT), when

it shifted back to an earlier time than -10% of the task range. This pattern corresponds well to that found in the transferred muscles (EDC; Fig. S3).

Again, the characteristics of these changes in activation coefficients of muscle synergies were also quantitatively confirmed by cross-correlation analysis of all four muscle synergies. The coefficients were plotted over the course of experimental days in relation to tendon surgery (Fig. 5). In this analysis, the activation coefficient of each synergy was cross-correlated with either the one from synergy A (finger flexor synergy; Fig. 5C, D, G, H) or synergy B (extensor synergy; Fig. 5A, B, E, F) before TT. As previously demonstrated for the FDS and EDC muscles, the temporal activation coefficients of muscle synergies A and B (flexor and extensor) displayed a distinct pattern. After cross-correlation with their own control data, both the flexor and extensor synergies showed coefficients of 1 prior to surgery. These became negative for 66 days post-surgery before reverting close to their original values (Fig. 5A, B). However, after cross-correlation with control data of the antagonistic muscle synergy (i.e., extensor for flexor synergy and vice versa), the pattern was reversed. Coefficients started with negative values prior to TT and shifted to positive coefficients near 1 shortly after surgery. Around 66 days later, the correlation coefficients returned to negative values. In short, these results mirror our findings between the transferred muscles (Fig. 3E, F). For synergies C and D, the changes in cross-correlation coefficients over time were markedly different. For synergy C, coefficients begin to steadily increase when cross-correlated with control data of the extensor synergy (synergy B), and decreased with the flexor synergy (synergy A). This suggests an increasing contribution to finger extension. In contrast, synergy D does not exhibit any specific pattern following TT. We also found a differential pattern of adaptation between transferred and non-transferred muscles in Monkey B (Fig. S12; Supplementary Text 1).

Overall, we observed early and late changes between two synergy pairs (synergy A and B) in both monkeys, performing controlled and natural grasping. Another characteristic change that reinforced finger extension in other synergies was also observed (i.e., synergy C in Monkey A).

Rationale for the early reverse and late switch-back changes

So far, our results suggest a two-step adaptation following TT: an early and a late phase. In the initial phase, as expected, the transferred muscles and their host

muscle synergies (activation coefficients) gained new functionalities. However, the later phase restored pre-TT EMG profiles and muscle synergies.

This two-step adaptation raises a key question: why? The early changes (where extensor muscles exhibited flexor properties and vice versa) seem reasonable and might be unique to CNS adaptation of non-human primates to TT. However, the later reversal seems puzzling. The monkeys were already performing the task well (Fig. S2). Why did the early adaptation need to switch back to the original pattern?

Here, we hypothesize that the TT forced the monkeys to explore new control strategies of both transferred and non-transferred muscles (early adaptation), and the reversing activity was a consequence of the monkey's exploitation of the previous strategy. This hypothesis assumes that the early adaptation was a "maladaptation" resulting from a now conflicting mechanical outcome of the agonistic muscles (i.e., transferred vs. non-transferred muscles). For example, the finger extensor synergy (synergy B) is composed of EDC, ED23, and ED45, and their combination remained unchanged after TT and recovery (Fig. 4B–E). However, the transferred EDC became an anatomical finger flexor, while ED23 and ED45 continued to be anatomical extensors. This led to paradoxical activation of synergistic muscles with the finger extension synergy having similar activity to the finger flexion synergy. Therefore, after early adaptation, monkeys needed to establish a novel strategy to control the altered musculoskeletal systems. Early maladaptation must have triggered this exploring process.

This hypothesis appears to be supported by two additional observations. First, we found unusual behavioral characteristics during target reaching and grasping after TT (Supplementary Videos 2, 3, and 6). We compared the kinematic performance of grasping during early adaptation, late adaptation, and pre-TT periods. Monkey A struggled significantly to lift its forearm towards the object, requiring either the experimenter's assistance or the use of its opposite arm as a support. It also performed 'explorative' finger movements over the object before finally grasping and pulling it, a process that took considerably longer than before TT (Video 2). Monkey B initially overshot and bumped into the object during the early adaptation period, but later managed to reduce and avoid this behavior (Video 6). These observations were further supported by measuring the time spent for this maladaptive behavioral component in both monkeys (Fig. S13). Monkey A exhibited malcoordinated reaching from day 29 (1978 ± 715 ms) to 73 (93.4 ± 3.7 ms) (see Methods for additional details). The duration decreased

progressively over time. Monkey B showed malcoordinated reaching from day 20 (103.4 ms) to 62 (107.6 ms). The duration peaked at days 38–46 (167 ±1.4 ms) and then declined. Notably, the periods dominated by malcoordinated movements coincided with the observed maladaptive swapping of synergy A and B activity, occurring between the early and late adaptation phases.

Second, we found that the net activity of muscles representing certain muscle synergies (aggregated average EMG; aaEMG) were unstable during the period between early (reversal) and late (switch-back) adaptation in their temporal activation patterns (Fig. 3). In Monkey A (Fig. 6; see Fig. S15 and Supplementary Text 2 for Monkey B), muscles of the finger flexor synergy (synergy A, Fig. 6A) tended to show a decrease in aaEMG post-TT, maintaining this lower activity level throughout the experiment ($p < 0.01$ at day 79, two-sample *t*-test, Bonferroni-corrected; $\alpha = 0.01$; panel E). Because the monkeys performed successful grasping after TT, this suggests that finger flexion is performed by muscles other than synergy A. The finger extensor synergy (synergy B, Fig. 6B) demonstrated a steady increase in aaEMG post-TT until day 64 ($p < 0.0001$, two-sample *t*-test, Bonferroni-corrected; $\alpha = 0.01$, panel F), when the activity abruptly reverted to near its pre-TT level. Increased activity of synergy B suggests a maladaptive attempt by the monkey to achieve finger flexion. This strategy involved enhancing activity of synergy B (which includes the EDC muscle, an atomical flexor) after TT. However, as previously established, this approach cannot effectively promote finger flexion, leading to eventual abandonment by the monkey.

Recruitment of novel, compensatory movements aiding finger extension

Muscles of synergy C (wrist flexion synergy) initially showed significantly decreased aaEMG post-TT (days 69 and 79: $p < 0.001$, two-sample *t*-test, Bonferroni-corrected; $\alpha = 0.01$, panel G) but then showed a gradual increase starting from day 64. This is consistent with the cross-correlation analysis (Fig. 5E), where cross-correlation coefficients between synergy C (wrist flexor) and synergy B (finger extensor) initially dropped post-TT but then first rapidly and then steadily increased over time. Increased reliance on synergy C following TT suggests a compensatory strategy to overcome the difficulty in finger extension, crucial for grasping. This is despite the recruitment of the finger extensor and wrist flexor synergies, which seemed inadequate to achieve effective flexion. The interactions between the cumulative proximal-to-distal joint angles and musculo-

tendon length can be complex. In our experiments, as in human patients who receive tendon transfers [22], those interactions can affect the ranges of finger flexion-extension that can be achieved for a given wrist angle (i.e., *passive and active tenodesis*). Briefly, biomechanically, wrist flexion can enable finger extension (i.e., a dynamic tenodesis where extensor tendons of the fingers cross both the wrist and interphalangeal joints): Finger extension can cancel out the increase in total musculo-tendon length produced by wrist flexion. This compensatory interaction across joints allows for some degree of functional hand use, even in the absence of active finger movement [23] (see the Discussion for a complete description).

Further kinematic analysis of Monkey B (Fig. S14; no analysis on Monkey A due to low-resolution video images) indicated that this monkey indeed exhibited a similar active tenodesis as human patients. The angle at the metacarpophalangeal (MCP) joint, responsible for finger extension, steadily increased (Fig. S14A) after surgery, indicating finger extension. Concurrently, the wrist joint angle decreased (Fig. S14B), indicating wrist flexion. This coordinated movement suggests a compensatory strategy to achieve finger extension during grasping. Statistical analysis confirmed that MCP and wrist joint angles differed significantly between pre- and post-TT ($p < 0.01$, ANOVA; $\alpha = 0.01$). Therefore, we suggest that deteriorated finger extension after TT was assisted by a compensatory wrist flexion synergy.

What triggered the late adaptation?

Assuming that TT caused maladaptation and forced the monkeys to explore new control strategies of both transferred and non-transferred muscles, what triggered the late adaptation and why did the grasping performance increase after this adaptation? To address this question, we summarized our experimental results in a simple model (Fig. 7) consisting of multiple adaptation processes to TT with different time constants: a *slow dynamics* adaptation and a *fast dynamics* adaptation. In this model, tendon cross-transfer surgery (black arrow) evoked changes in coordination of finger muscle activity (i.e., swapping temporal activity of flexor and extensor synergies; left blue arrow). These changes were sufficient to reach a threshold (blue dotted line) and trigger (arrow 1) adaptation with slow dynamics (A and B). This slow process may have different time constants. For example, synergy B (Monkey A), which comprises EDC and ED23/ED45, consistently elevated its activity to achieve successful flexion after TT (red line

“A”). This ‘arms race’ is instigated by conflicting activation of the ‘new flexor’ (EDC) and its previous agonists (ED23/45), which still mechanically function as finger extensors. In contrast, synergy A can reduce its activity as synergy D (containing FDP), and accomplish the necessary finger flexion by simply adjusting its timing (Figs. 4, S4, and S6), thereby circumventing the ‘arms race’. However, this ‘arms race’ observed in synergy B can only persist until a second threshold (red dotted line) is reached, whereby a further increase in muscle activity becomes unsustainable. At this point, the second fast adaptation process (blue arrow i.e., switch-back) is recruited, allowing the monkeys to cease flexing their fingers by excessive activation of synergy B, thus concluding the ‘arms race”. Meanwhile, an alternative, sustainable strategy to perform finger extension has been developed (Fig. S14). Specifically, the monkey increasingly recruited synergy C (wrist flexors, PL and FCR) to aid finger extension using the tenodesis effect (wrist flexion), which was more effective after the ‘arms race’ was concluded. These implications can also be applicable to Monkey B (Supplementary Text 2).

DISCUSSION

In our cross-union TT model, we identified three distinct modes of CNS adaptation, each distinguished by their characteristic time course. Notably, changes involving the relocated muscles (FDS and EDC) and their synergists (synergy A and B) exhibited rapid alterations within a few days, during both the early and later phases of adaptation. We propose that the early changes are maladaptive, while the later change represent a “good enough” adaptation. In addition, changes involving certain non-relocated muscles were slower and more gradual throughout the adaptation period, suggesting a compensatory role. These slower adaptations appear to mitigate maladaptive responses and contribute to improved performance after achieving a “good enough” adaptation, possibly through exploitation of an active tenodesis effect. We will first explore the potential causes of this distinct adaptation in relocated versus non-relocated muscles, followed by a discussion on the potential interactions between these different adaptation modes.

Relocated muscles and their synergists: early and late adaptation

The most straightforward way for the CNS to adapt control of relocated muscles (e.g., FDS and EDC) is to simply swap control strategies. In theory, this means the FDS EMG activity pattern would then mimic the original EDC EMG pattern, or vice versa. However, our observations exceeded our expectations. We found that temporal activation of the relocated muscles’ host synergies (synergy A and B) were also swapped, not just the relocated muscles themselves.

This suggests that selectively altering the activity of a single muscle within a strongly co-activated muscle group poses a significant challenge for the CNS [24, 25], as the EDC and FDS are coactive with their synergist extensor and flexor wrist muscles [26]. This also implies that a majority of muscle activity in daily life could be generated through the CNS module responsible for coactivation, rather than the higher motor centers dedicated to controlling individual muscles [27]. Consequently, the CNS opted to swap temporal activation of the muscle synergy, leaving the synergy itself unchanged.

However, this initial adaptation turned out to be maladaptive. It involved muscles unaffected by the TT, leading to a steady increase of antagonistic muscle activity and thus antagonistic proprioceptive feedback in the non-transferred muscles over time. Notably, temporal activation of these synergies reverted to their original

pattern during the late adaptation period. The now reversed but decreased antagonistic activity might be a “good enough” solution because the antagonism now stems from only two muscles, i.e., the transferred muscles EDC and FDS. Adaptation in the non-transferred muscles and their synergists could potentially compensate for this remaining antagonism.

Both these initial maladaptive and later switch-back changes occurred within a few days, suggesting a rapid CNS response. Although the underlying CNS mechanisms for this rapid response remain unclear, we hypothesize that different mechanisms might be involved in the initial and later rapid response.

The initial response could be linked to the ‘sensory surprise’ induced by the surgery [28]. The muscle relocation essentially presented the animal with a new internal, proprioceptive environment. Motor commands intended to generate flexor activity resulted in extensor proprioceptive feedback from the transferred muscle, similar to the reversed prism paradigm [29-31]. We speculate that this unexpected sensorimotor mismatch served as a strong driver, prompting rapid CNS adaptation to minimize prediction errors [32, 33], but that ultimately led to maladaptation.

Previous studies have shown that motor learning is often characterized by non-linearity and a tendency towards “good enough” solutions [34, 35]. When faced with challenges, animals prioritize minimizing effort over achieving optimal performance. This is evident in human motor control, where individuals often learn to exploit redundancy in movement to reduce costs. For example, in a cursor-control task, participants developed distinct hand postures to reach the same target, depending on their starting position. This adaptive strategy allowed minimization of movement-related costs by effectively utilizing the available degrees of freedom [36]. In our study, eventual return to the original activation pattern, despite some residual antagonistic activity, suggests a similar optimization strategy. The nervous system may prioritize reducing overall effort over achieving perfect efficiency, even if it means compromising on precision.

Slow and gradual adaptation of several non-relocated muscles

We observed slower and gradual changes in EMG activity of muscles not belonging to synergies of the relocated muscle’s (e.g., FDP, ECR, PL, and FCR in Monkey A, Fig. S4). This is in stark contrast to the rapid adaptation discussed earlier, suggesting a distinct CNS mechanism. One example of this slow adaptation is the gradual development of a compensatory wrist flexion to

substitute for the reduced extensor function of the finger. This compensatory motion helps to make the affected movement by activating unaffected muscles. Indeed, this may be analogous with common clinical observations (e.g., paralyzed stroke patients exhibiting assistive shoulder abduction [37], trunk movement [38], or activation of posterior trunk muscle synergies [39] for producing upper arm movements). In our study, this involved a muscle synergy (synergy C in Monkey A, and synergy A in Monkey B) primarily composed of wrist flexors (FCR and PL). Notably, activity of these muscles, along with temporal activation of their host synergy, increased throughout the experimental period, particularly before grasping (Figs. S6Q, S and S11C; and S7R and S11A; for Monkeys A and B, respectively). This wrist flexion activity helps with pre-shaping the fingers (extension) before grasping [40]. Successful replication of this clinically known active tenodesis effect in our experiment suggests this slow adaptation process is not specific to the TT model of our study, and could potentially be generalized to other TT models in spinal cord injury, and even other clinical scenarios such as stroke rehabilitation [41, 42]. For instance, Raghavan and colleagues [43] demonstrated compensatory hand use in stroke patients with hemiparesis. Patients showed greater reliance on MCP flexion for grasping objects compared with healthy controls who used more proximal interphalangeal (PIP) flexion. Additionally, their hand shaping was delayed and finger movements were reduced. They could, however, still differentiate hand postures for different object shapes, suggesting partial effectiveness of their compensatory strategy.

Another type of slow adaptation was observed in the EMG activity of FDP, the core finger flexor essential for finger grasping. Before surgery, lever pulling was primarily achieved by FDS activation, and the role of FDP was mainly for holding, not pulling, the object [44]. As discussed earlier, during the initial adaptation phase, FDS swapped its activity pattern with EDC. Later, it switched back. Interestingly, FDP maintained its original activity pattern throughout the experiment but gradually increased its activity without reverting to its original timing. This change in FDP activity appeared independent of the temporal activation changes in its host synergy (synergy D). Indeed, the activity of FDS appeared to merge into FDP activity after TT (Figs. S4P and S6M). This suggests a potential alteration in the synergy itself, although we found no drastic changes in synergy composition after TT. Although the underlying CNS mechanism remains unclear, these findings suggest that reorganizing muscle synergies, or

acquiring a novel activity control pattern for a single muscle independent of its synergist, takes a longer time due to a slower adaptation process.

Neural adaptation from different adaptive modules

A fascinating question emerges: do the rapid and gradual adaptation processes following muscle relocation function independently, or do they interact with each other? Our model summarizing our results (Fig. 7) supports the latter possibility. An acute change in the musculoskeletal system, such as by TT, inevitably generates a sensory prediction error (SPE). For example, in our experiment, we cross-transferred two muscles with vastly different mechanics: a finger flexor and extensor. In this case, proprioceptive feedback is predicted from the flexor muscle during grasping, but instead is perceived as finger extension. The magnitude of SPE can vary depending on the extent of differences in functionality of the transferred muscles. The SPE might be smaller or even negligible when transferring muscles with similar mechanical actions (e.g., synergistic muscles). We hypothesize that this SPE drives the CNS to adopt a sensorimotor control strategy to minimize it. When SPE is small (below the threshold indicated by the blue line in Fig. 7), the CNS employs a slower adaptation strategy that involves a gradual adjustment to the motor command. Monkeys can still perform tasks during this slow adaptation because the required motor commands are not significantly different before and after the bodily change.

In contrast, for larger SPEs (above the threshold in Fig. 7), a slower adaptation process alone might not be sufficient to overcome the error without impacting task performance, as observed in our study. Consequently, the CNS first recruits a fast adaptation process, which is necessary for quick and drastic changes, although it may not be the most efficient. In this study, the initial response of the CNS to TT was to swap extensor and flexor synergies, which is a drastic but theoretically flawed approach (i.e., maladaptation).

Although this initial, slow adaptation “resets” the large SPE, it likely generates a new, and potentially larger, SPE (due to more muscles producing conflicting sensory feedback). From this new baseline state, the CNS employs a slow adaptation process again to “explore” the optimal sensorimotor commands and minimize this SPE. In our case, fast maladaptive changes triggered the recruitment of at least two distinct slow processes (A and B) to minimize the new SPE. Process A aimed to maintain the outcome of fast adaptation, but could not actually reduce SPE because it was a maladaptation. Consequently, the CNS

essentially continued augmenting the maladaptive motor signal, seemingly desensitized to the fact that there was no decrease in the SPE. Conversely, process B aimed to construct a new behavior to perform the task more smoothly. Since this novel behavior ("compensatory movement") is tailored to the altered body, the associated SPE should be minimal compared to the maladaptive behavior.

The slow adaptation process (A) eventually triggers recruitment of a second fast adaptation in the later period. The timing of this might coincide with the cumulative cost of using the maladaptive behavior until it reaches its threshold (red dotted line). This triggered fast adaptation serves two purposes: first, to stop using the maladaptive behavior and revert to the original motor control strategy; and second, to explicitly use the novel behavior, which can compensate for antagonism between the transferred and non-transferred muscle activity. While some SPE might still exist due to this antagonism, it can be considered a "good enough" solution [36] since the monkeys can now perform the behavior more smoothly without significant SPE.

Implication for sensorimotor rehabilitation

Our findings hold significant implications for potential rehabilitation programs. A staged approach could be beneficial, with an early phase focusing on minimizing SPEs through techniques like mirror therapy or visual feedback training [45, 46]. This could include repetitive practice with augmented reality or biofeedback to reinforce desired motor commands [47, 48], and task-oriented practice with progressive challenges and error tolerance [49]. This may help the nervous system integrate the altered body schema and reduce initial maladaptive responses [50-52]. Notably, Izawa and colleagues [53] suggest that these early rehabilitation exercises might also lay the groundwork for later re-learning of the original skill through a process of neural generalization [54-57].

Alternatively, a later phase could introduce task-specific training to promote the development of compensatory strategies and encourage muscle synergy reorganization, similar to the slow adaptation observed in non-relocated muscles [58]. Thus, practicing these compensatory strategies could actually benefit re-learning of the original skill. This aligns with the observation that the nervous system eventually abandons the maladaptive strategy in favor of the original skill [59].

METHODS

Animals

Data were collected using two male macaque monkeys (*Macaca fuscata*; Monkey A: 7.8 kg and Monkey B: 9.9 kg) purpose-bred at the National Bioresource Project (NBRP). They were kept in custom-made primate cages, allowing for potential pair housing. Both monkeys were trained to perform a simple grasping task. During experimental recordings, the monkeys were seated in a primate chair without further restraint. Their head movement remained unrestricted at all times.

Procedures

All procedures were designed to minimize discomfort and pain and approved by the institutional Animal Care and Use Committees at the National Center of Neurology and Psychiatry (NCNP), Tokyo, Japan. Details of the surgical operations, experimental setup, and procedures for electromyography (EMG) recordings have been previously described [60].

Surgery

Both animals were familiarized with the experimental setup and trained to perform the behavioral task prior to surgery. After an initial training period, EMG electrodes were chronically implanted subcutaneously into several muscles of the left forearm including the FDS, FDP, and EDC (Figs. 1A, 2C, and S1C). Individual muscles were localized and confirmed using electrical microstimulation before implanting EMG electrodes chronically by two methods. For muscles involved in the tendon cross-union procedure, muscle fascia was cut and EMG wires with looped ends were placed on top of the muscle belly. These were then secured by reclosing the fascia with absorbable suture threaded through the loop (AS-361, stainless-steel Cooner wire, Conner Wire Co., Chatsworth, CA, USA). All other muscles were directly implanted into the muscle belly using a 22-gauge hypodermic needle. Each wire was threaded into the needle tip, folded back along the shaft, and inserted into the muscle before carefully retracting the needle. Electrode separation for bipolar recordings was approximately 5–10 mm. Note that some EMG recording sites were lost over time.

After a minimum four-week recovery period, TT surgery was performed. The FDS and EDC tendons were cut as distally as possible (immediately below and above the wrist for FDS and EDC, respectively) to avoid damaging the Golgi tendon

organ located near the junction between the muscle fibers and tendon [61, 62]. Tendons were then guided either through the gap between the radius and ulnar bone (Monkey A), or around the wrist and then re-attached to the tendon of the antagonist muscle using a tendon graft harvested from the plantaris tendon of the lower limb (Monkey B; EDC → FDS: direct connection; and FDS → EDC: tendon grafting). This was only necessary in Monkey B since the tendons used for the cross-transfer were too short.

Surgical procedures were carried out under deep general anesthesia (sevoflurane 1.5 to 2.5% in 2:1 O_2/N_2O) and with full aseptic precautions. Heart rate, blood pressure, body temperature, and blood oxygen saturation were monitored throughout surgery. Analgesics and antibiotics were administered intramuscularly for at least one week postoperatively. Both monkeys wore a plaster cast post-surgery, but its effectiveness was limited (lasting approximately one week).

Tendon transfer confirmation

To verify the success and long-term stability of TT surgery, two procedures (Fig. 1B–G) were implemented. During the first procedure, the monkey was sedated and its arm was secured to a metal frame (Fig. 1B). Electrical stimulation was then applied to either the FDS or EDC muscle (50 mA, DS8R, Digitimer, Welwyn Garden City, UK), while ultrasound scans of tendon movements were concurrently captured (SONIMAGE MX1, Konica Minolta, Inc., Tokyo, Japan [63, 64]).

Figure 1C shows a sonogram of the FDS muscle and its intramuscular tendons. The left side displays a static image of the FDS muscle at a specific moment, with white arrows indicating the FDS tendon used for measurement. The right side shows staggered images (top white box) of the FDS tendon displacement triggered by muscle stimulation. The lower right inset illustrates the measurement area. The displacement wave area represents the intensity of muscle contraction, and was calculated by measuring the average duration (a, in seconds) and amplitude (b, in cm) of three successive waves. The area (a*b/2) and regression line for FDS (red) and EDC (blue) ($R^2 > 0.5$ for FDS) for days 0, 7, and 105 post-TT are shown (Fig. 1D). The results suggest that the muscle contractions induced by direct electrical stimulation remained nearly constant.

For the second procedure, high-speed videos (37U Series Color Industrial Camera, The Imaging Source, Charlotte, NC, USA) of the monkey’s finger

movements were recorded while electrically stimulating the FDS or EDC. Markers were placed on the nails of the index, middle, and ring fingers (Fig. 1B) to measure finger displacement in xyz-dimensions using DeepLabCut software [65, 66]. The sum of Euclidean distances of each marker from the origin of the three-dimensional (3D) coordinate system was computed as a scalar quantity. Post-surgery, movement along the z-axis reversed, indicating a shift from finger flexion to extension due to TT (Fig. 1E; blue: pre-TT on surgery day, dark brown: post-TT on surgery day, light brown: 1 wk post-TT, and red: 3 wk post-TT). The scalar quantities of each finger did not significantly change during muscle stimulation on days 0-, 7-, and 105-days post-TT (Fig. 1F, G), suggesting there was no postoperative tendon rupture or slackening.

Behavioral task

Before and after EMG surgery, the monkeys were trained on a simple grasping task that involved a small object attached to a rod (Fig. 2B for Monkey A; and Fig. S1B for Monkey B). For Monkey A, object 1 was a small rod placed between two side walls encouraging the monkey to grasp the rod with a precision grip using the tips of the index finger and thumb (controlled grasp). The force used to compress the spring while pulling was low and the distance moved short. Object 2 had to be grasped in the same way. However, the force to compress the spring was higher and the distance moved longer (object 1: 300 cN, 4 mm; and object 2: 800 cN, 30 mm). The monkey was asked to grasp and hold the objects for approximately 300–500 ms (Fig. 2A–D). After completing the trial, the monkey was rewarded with a piece of fruit that had to be taken from the experimenter's palm. The task sequence for Monkey A ranged from object 1 hold onset to object 2 hold offset (Fig. 2C, D; and 'Data Analysis' below). For Monkey B, object 1 was a small rod that was grasped and pulled (300 cN, 4 mm) using a lateral prehension grip (like using a door key), and resembling a power grip rather than a natural grasp. However, instead of grasping object 2, Monkey B picked up a piece of fruit from an allocated location. In doing so, the monkey had to cross the path of a photo cell which was detected by the recording system (Fig. S1A–D). The task sequence to be analyzed for Monkey B ranged from object 1 hold onset to food touch, which was indicated by a LED (Fig. S1C, D; and 'Data Analysis' below).

For Monkey A, the task sequence was as follows (Fig. 2A; and Supplementary Video 1). From a starting position in front of the monkey, it had to lift its arm and

move towards object 1, grasp, pull, and then hold the object for 500 ms. Immediately after releasing object 1, Monkey A proceeded to move its hand towards object 2, which was located to the right of object 1. Again, the monkey had to grasp, pull, and then hold the object for another 500 ms. Each hold period was accompanied by an audio signal which stopped once the hold duration was sufficient. After completing the task, which was signaled by another acoustic signal, the monkey was rewarded with a piece of fruit presented by the experimenter and taken by the monkey.

For Monkey B, the first part of the sequence was identical. However, after releasing object 1, Monkey B was required to pick up a piece of fruit from an allocated location (Fig. S1A, B; and Supplementary Video 5). In doing so, the monkey passed a photocell in front of the food well. This event was detected by the recording system and a video camera (a red LED triggered by activation of the photocell). For the analysis, only object 1 and the food grasp were considered in monkeys A and B, respectively.

Data recordings

EMG signals were recorded using the AlphaLab SnR system (Alpha Omega Engineering, Hamerkava St. 6, Ziporit Industrial Zone, P.O.Box 810, Nof HaGalil (Nazareth Illit) 1789062, Israel), displayed online and then stored on a hard drive for later off-line analysis using MATLAB (MathWorks, Natick, MA, USA). Data were recorded at 11 kHz and processed for analysis as follows. 1. Down-sampled to 5 kHz; 2. 50 Hz high-pass filtered (6th order Butterworth filter); 3. rectified; 4. 20 Hz low-pass filtered (6th order Butterworth filter); and 5. down-sampled to 100 Hz. Behavioral task events were recorded as transistor–transistor logic (TTL) signals using the AlphaLab SnR system. Monkey behavior was further recorded by two cameras (Sanyo VPC-WH1, 60 fps [Sanyo, Osaka, Japan]; and Casio EX-100F, 240 fps [Casio, Tokyo, Japan] for monkeys A and B, respectively) from two different angles (top and side view). The images were later used to detect additional behavioral events (contact time with the object and pull onset for Monkey A; and food touch and food lift onset for Monkey B), and detection of possible changes in the animal's general movement pattern. Kinovea software was used for this video analysis (free and open-source software; https://www.kinovea.org/).

Data analysis

EMG analysis

EMG data were normalized to the average time for each monkey to complete a trial (object 1 hold onset ➔ object 2 hold offset/LED offset = 100%). Data were cropped and aligned according to the time stamps (Obj1 hold offset ± 15%; and LED onset [food touch] ± 15% for monkeys A and B, respectively). Recorded EMGs from the pre- and post-tendon surgery period were averaged for each recording and compared over experimental sessions. For both monkeys, the muscles used for EMG analysis were: FDS and EDC for pre- (control) and EDC for post-TT (experimental).

Both monkeys required time to recover from surgery. Once they were able to perform the task on their own, data collection started (29 and 20 days post-surgery for monkeys A and B, respectively). After tendon surgery, EMG signals for FDS, FCU, and FCR deteriorated in Monkey B. Therefore, there is no experimental data for these muscles in this monkey and they were excluded from the muscle synergy analysis.

Synergy analysis

The EMG envelopes obtained from pre-processing raw EMG data were divided by the mean value to normalize activity. Muscle synergies were then extracted for each session using NMF [67]. NMF decomposes the EMG data matrix *M*, as a product of two matrices *C* and *W*:

$$M = CW^T + re = \Sigma c_i {w_i}^T + re$$

where the vector *wi* and column of matrix *W* are muscle synergies; the vector *ci*, and column of matrix *C* are their temporal coefficients; and *re* represents the residuals. Multiplicative update rules were used for decomposition [20]. Updating matrices for decomposition from 20 different random initial matrices was started, and factorization results with least residuals among the 20 results were used. To improve robustness of the muscle synergies, one set of muscle synergies was extracted from EMG data of multiple trials of each day. A *k*-fold cross validation was used, with *k* = 4 i.e., EMG data set of multiple trials during the day was split into four data sets, in which three data sets were for training and one data set was for testing. Synergy matrix *W* was calculated from three training data sets using NMF, and then a coefficient matrix *C* was calculated by decomposing the

EMG matrix *M* of the test data set with a fixed *W* matrix of the training data set. This operation was repeated by changing the test data set for each four data sets. Finally, the extracted four *C* matrices and four *W* matrices were averaged to obtain daily synergies.

The number of synergies was determined as the number where VAF exceeded a threshold. This threshold was set as 0.8. To clarify the effect of TT, the number of synergies for each monkey was determined, assuming that trial-by-trial variation in synergies within the same monkey was small. MATLAB 'nnmf' function was used for NMF.

To determine whether the weights of muscle synergies changed after TT, the following procedure was used. First, the average of each pre-TT spatial synergy was calculated and used as control data to calculate the cosine distance for all post-TT spatial synergies. This generated four distance relationships for each pre-TT synergy. If the change in spatial synergy before and after TT was small, then only one of the four cosine distances (e.g., synergy A before TT and synergy A after TT) should be significantly smaller. Two-way ANOVA was conducted using the type of synergy and session as factors for the cosine distance. The significance of synergy pairs was identified using the Bonferroni post-hoc test.

Cross-correlation analysis

Cross-correlation analysis was performed to examine pre- and post-surgery EMG signals as well as temporal activation coefficients of extracted muscle synergies. Cross-correlation coefficients were calculated using MATLAB (MathWorks, corrcoef.m function). These were plotted for different muscles and muscle synergy activation coefficients over experimental sessions for comparison.

Based on cross-correlation analysis (Figs. 3E, F, and S3D), five 'landmark days' were identified for further analysis (Figs. 3E, F, and S3D). These days represent distinct stages in the recovery process and excluded pre-surgery control data. The first landmark day was chosen from one of the initial recording sessions after TT surgery (days 29 and 22 in monkeys A and B, respectively) when the cross-correlation coefficients had changed significantly compared with control data. The second day was then chosen from a time period just before the switch-back, when the cross-correlation coefficients had started to return to their original values (days 64 and 36). Another day was then picked from the period when the coefficients were still changing significantly (days 69 and 44) and before starting

to saturate. At this point the next day was defined (days 79 and 48). Finally, the final landmark day was chosen from one of the last recording sessions when the behavior had fully recovered (days 99 and day 64 for monkeys A and B, respectively).

Behavioral analysis

To examine behavioral recovery, the duration, onset, and offset of object and food grasps were analyzed. Event times extracted from the video analysis were used for alignment of EMG data and subsequent cross-correlation and synergy analyses, along with recorded event TTL signals. For each experimental session, the first 20 trials of each video recording were analyzed. In Monkey A, the following events were detected and in-between times stored in ms: touch onset, pull onset, and hold onset (resulting in grasp duration and pull time) for object 1 and object 2. In Monkey B, the following events were detected and in-between times stored: touch onset, pull onset, and hold onset (resulting in grasp duration and pull time) for object 1; and for the food grasp component of the task, LED onset, food-touch onset, food-lift onset, LED offset, and movement end (contact of food with mouth).

Contact times (touch onset ➔ pull onset) for Monkey A were plotted in ms (mean ± SD) over number of days from tendon surgery for object 1. For Monkey B, contact times with food (food-touch ➔ food-lift onset) were plotted in ms (mean ± SD).

ANOVA was performed to compare control data recorded before and after tendon surgery. In total, 5 and 3 control sessions vs. 35 and 22 experimental sessions were used for analyses in monkeys A and B, respectively.

To quantify the observed malcoordinated reaching behavior, video footage was analyzed and the means of 10 consecutive trials calculated for each session as follows. For Monkey A, time spent within a specific spatial window covering the area behind and between the two objects was measured; the monkey passed through this space almost exclusively while exhibiting the impairment (see Fig. 2E, crossing of the yellow dotted line). In Monkey B, the time spent in contact with the rear plate of the object was measured (see Fig. S1G).

Joint kinematics analysis

To determine whether compensatory movements occurred, steady state changes in joint angles were examined before and after recovery. Using DeepLabCut [65, 66], key points on the fingers and wrists were tracked from experimental videos. From the obtained key points, the vector v_1 connecting the wrist and fingers and vector v_2 connecting the arm and wrist were estimated. The joint angle θ was calculated as follows:

$$cos(\Theta) = \frac{\underline{v}_2 \cdot \underline{v}_3}{|\underline{v}_2|\,|\underline{v}_3|} \rightarrow \Theta = cos^{-1}\left(\frac{\underline{v}_2 \cdot \underline{v}_3}{|\underline{v}_2|\,|\underline{v}_3|}\right)$$

ACKNOWLEDGEMENTS:

We would like to express our sincere gratitude to Drs. Francisco Valero-Cuevas and Andrea d'Avella for their invaluable comments and constructive suggestions on the earlier version of the manuscript, and Drs Nicholas Schweighofer and Gerald E. Loeb for stimulating discussion. We would also like to thank Dr. Naomichi Ogihara and Prof. Toshiyasu Nakamura for their valuable insights and technical advice on tendon surgery in the hand and forearm of primates. We are grateful to Drs. Kumiko Oida and Chika Sasaki for their medical care of the experimental animals, vital help during surgery, and training of the animals. Lastly, we would like to thank Masahi Koizumi for designing parts of the experimental setup and Drs. Joachim Confais, Shinji Kubota, Saeka Tomatsu, Tatsuya Umeda, and Natsumi Uchida for their support and assistance during the proceeding pilot study. We thank Rachel James, PhD, from Edanz (https://jp.edanz.com/ac) for editing a draft of this manuscript.

This work was supported by Grants-in-Aid for Scientific Research from the Ministry of Education, Culture, Sports, Science, and Technology of Japan (26120003, 26250013, 15K21754, 19H05724, 19H01092, 23H05488, and 24K21313), the Japan Agency for Medical Research and Development (JP24gm0010009), the Japan Science Technology Agency Precursory Research for Embryonic Science and Technology program, commissioned research (no. 22102) from the National Institute of Information and Communications Technology, and commissioned research by National Institute of Information and Communications Technology (NICT), Japan (all to K.S.). This work is also supported in part by the NSF CRCNS Japan-US 2113096 to K.S. (Subaward PI) and Francisco Valero-Cueva (PI). The content is solely the responsibility of the authors and does not necessarily represent the official views of the NSF.

DATA, MATERIALS, AND SOFTWARE AVAILABILITY

Matlab scripts and raw data will be made available online. All study data are included in the article and/or SI Appendix.

REFERENCES

1. Power, J.D. and B.L. Schlaggar, *Neural plasticity across the lifespan.* Wiley Interdisciplinary Reviews: Developmental Biology, 2017. **6**(1): p. e216.
2. Fleury, L., C. Prablanc, and A.-E. Priot, *Do prism and other adaptation paradigms really measure the same processes?* Cortex, 2019. **119**: p. 480-496.
3. Sugita, Y., *Global plasticity in adult visual cortex following reversal of visual input.* Nature, 1996. **380**(6574): p. 523-6.
4. Luauté, J., et al., *Dynamic changes in brain activity during prism adaptation.* J Neurosci, 2009. **29**(1): p. 169-78.
5. Li, C.S., C. Padoa-Schioppa, and E. Bizzi, *Neuronal correlates of motor performance and motor learning in the primary motor cortex of monkeys adapting to an external force field.* Neuron, 2001. **30**(2): p. 593-607.
6. Davidson, P.R. and D.M. Wolpert, *Motor learning and prediction in a variable environment.* Curr Opin Neurobiol, 2003. **13**(2): p. 232-7.
7. Green, H.J., *Mechanisms of muscle fatigue in intense exercise.* J Sports Sci, 1997. **15**(3): p. 247-56.
8. Zemková, E., *Physiological Mechanisms of Exercise and Its Effects on Postural Sway: Does Sport Make a Difference?* Front Physiol, 2022. **13**: p. 792875.
9. Schärli, A., et al., *How spotting technique affects dizziness and postural stability after full-body rotations in dancers.* Hum Mov Sci, 2024. **95**: p. 103211.
10. Walker, J.G., H.J. Jackson, and G.O. Littlejohn, *Models of adjustment to chronic illness: using the example of rheumatoid arthritis.* Clin Psychol Rev, 2004. **24**(4): p. 461-88.
11. Sperry, R.W., *The functional results of muscle transposition in the hind limb of the rat.* Journal of Comparative Neurology, 1940. **73**(3): p. 379-404.
12. Sperry, R.W., *Transplantation of motor nerves and muscles in the forelimb of the rat.* The Journal of Comparative Neurology, 1942. **76**(2): p. 38.
13. Slawinska, U. and S. Kasicki, *Altered electromyographic activity pattern of rat soleus muscle transposed into the bed of antagonist muscle.* J Neurosci, 2002. **22**(14): p. 5808-12.
14. Bowlus, T.H., et al., *Comparison of reorganization of the somatosensory system in rats that sustained forelimb removal as neonates and as adults.* J Comp Neurol, 2003. **465**(3): p. 335-48.
15. Yumiya, H., K.D. Larsen, and H. Asanuma, *Motor readjustment and input-output relationship of motor cortex following cross-connection of forearm muscles in cats.* Brain Res, 1979. **177**(3): p. 566-70.
16. Loeb, G.E., *Asymmetry of hindlimb muscle activity and cutaneous reflexes after tendon transfers in kittens.* J Neurophysiol, 1999. **82**(6): p. 3392-405.
17. Gaetz, W., et al., *Massive cortical reorganization is reversible following bilateral transplants of the hands: evidence from the first successful bilateral pediatric hand transplant patient.* Ann Clin

975 Transl Neurol, 2018. **5**(1): p. 92-97.
976 18. Gaetz, W., et al., *Somatosensory and motor representations following bilateral transplants of the*
977 *hands: A 6-year longitudinal case report on the first pediatric bilateral hand transplant patient.*
978 Brain Res, 2023. **1804**: p. 148262.
979 19. Wester, K., et al., *Cortical Plasticity After Surgical Tendon Transfer in Tetraplegics.* Front Hum
980 Neurosci, 2018. **12**: p. 234.
981 20. Lee, D.D. and H.S. Seung, *Learning the parts of objects by non-negative matrix factorization.*
982 Nature, 1999. **401**(6755): p. 788-91.
983 21. Cheung, V.C., et al., *Muscle synergy patterns as physiological markers of motor cortical damage.*
984 Proc Natl Acad Sci U S A, 2012. **109**(36): p. 14652-6.
985 22. Zajac, F.E., *How musculotendon architecture and joint geometry affect the capacity of muscles to*
986 *move and exert force on objects: a review with application to arm and forearm tendon transfer*
987 *design.* J Hand Surg Am, 1992. **17**(5): p. 799-804.
988 23. Cash, D.J.W. and J.W.M. Jones, *The role of tenodesis in surgery of the upper limb.* The Journal of
989 Bone & Joint Surgery British Volume, 2011. **93-B**(3): p. 285-292.
990 24. Overduin, S.A., et al., *Modulation of muscle synergy recruitment in primate grasping.* J Neurosci,
991 2008. **28**(4): p. 880-92.
992 25. Berger, D.J., et al., *Differences in Adaptation Rates after Virtual Surgeries Provide Direct Evidence*
993 *for Modularity.* The Journal of Neuroscience, 2013. **33**(30): p. 12384-12394.
994 26. Madarshahian, S. and M.L. Latash, *Reciprocal and coactivation commands at the level of*
995 *individual motor units in an extrinsic finger flexor-extensor muscle pair.* Exp Brain Res, 2022.
996 **240**(1): p. 321-340.
997 27. Takei, T., et al., *Neural basis for hand muscle synergies in the primate spinal cord.* Proceedings of
998 the National Academy of Sciences, 2017. **114**(32): p. 8643-8648.
999 28. Edwards, M.J., et al., *A Bayesian account of 'hysteria'.* Brain, 2012. **135**(Pt 11): p. 3495-512.
1000 29. Kitazawa, S., T. Kohno, and T. Uka, *Effects of delayed visual information on the rate and amount*
1001 *of prism adaptation in the human.* J Neurosci, 1995. **15**(11): p. 7644-52.
1002 30. Martin, T.A., et al., *Throwing while looking through prisms. I. Focal olivocerebellar lesions impair*
1003 *adaptation.* Brain, 1996. **119 (Pt 4)**: p. 1183-98.
1004 31. Martin, T.A., et al., *Throwing while looking through prisms. II. Specificity and storage of multiple*
1005 *gaze-throw calibrations.* Brain, 1996. **119 (Pt 4)**: p. 1199-211.
1006 32. Smith, M.A., A. Ghazizadeh, and R. Shadmehr, *Interacting adaptive processes with different*
1007 *timescales underlie short-term motor learning.* PLoS Biol, 2006. **4**(6): p. e179.
1008 33. Petitet, P., J.X. O'Reilly, and J. O'Shea, *Towards a neuro-computational account of prism*
1009 *adaptation.* Neuropsychologia, 2018. **115**: p. 188-203.
1010 34. Gijsberts, A., et al., *Stable myoelectric control of a hand prosthesis using non-linear incremental*

learning. Front Neurorobot, 2014. **8**: p. 8.

35. Mussa-Ivaldi, F.A. and E. Bizzi, *The Modular Organization of Motor Control: What Frogs Can Teach Us About Adaptive Learning.* IFAC Proceedings Volumes, 1995. **28**(15): p. 413-418.
36. Ranganathan, R., A. Adewuyi, and F.A. Mussa-Ivaldi, *Learning to be lazy: exploiting redundancy in a novel task to minimize movement-related effort.* J Neurosci, 2013. **33**(7): p. 2754-60.
37. Lee, M.Y., et al., *Cortical activation pattern of compensatory movement in stroke patients.* NeuroRehabilitation, 2009. **25**(4): p. 255-60.
38. van Kordelaar, J., E.E. van Wegen, and G. Kwakkel, *Unraveling the interaction between pathological upper limb synergies and compensatory trunk movements during reach-to-grasp after stroke: a cross-sectional study.* Exp Brain Res, 2012. **221**(3): p. 251-62.
39. Funato, T., et al., *Muscle synergy analysis yields an efficient and physiologically relevant method of assessing stroke.* Brain Commun, 2022. **4**(4): p. fcac200.
40. McFarland, D.C., et al., *A Musculoskeletal Model of the Hand and Wrist Capable of Simulating Functional Tasks.* IEEE Trans Biomed Eng, 2023. **70**(5): p. 1424-1435.
41. Jones, T.A., *Motor compensation and its effects on neural reorganization after stroke.* Nature Reviews Neuroscience, 2017. **18**(5): p. 267-280.
42. Cirstea, M.C. and M.F. Levin, *Compensatory strategies for reaching in stroke.* Brain, 2000. **123 (Pt 5)**: p. 940-53.
43. Raghavan, P., et al., *Compensatory motor control after stroke: an alternative joint strategy for object-dependent shaping of hand posture.* J Neurophysiol, 2010. **103**(6): p. 3034-43.
44. Brochier, T., et al., *Patterns of muscle activity underlying object-specific grasp by the macaque monkey.* J Neurophysiol, 2004. **92**(3): p. 1770-82.
45. Foell, J., et al., *Mirror therapy for phantom limb pain: brain changes and the role of body representation.* Eur J Pain, 2014. **18**(5): p. 729-39.
46. Sattin, D., et al., *An Overview of the Body Schema and Body Image: Theoretical Models, Methodological Settings and Pitfalls for Rehabilitation of Persons with Neurological Disorders.* Brain Sci, 2023. **13**(10).
47. Levin, M.F., P.L. Weiss, and E.A. Keshner, *Emergence of virtual reality as a tool for upper limb rehabilitation: incorporation of motor control and motor learning principles.* Phys Ther, 2015. **95**(3): p. 415-25.
48. De Nunzio, A.M., et al., *Relieving phantom limb pain with multimodal sensory-motor training.* J Neural Eng, 2018. **15**(6): p. 066022.
49. van Vliet, P., et al., *Task-specific training versus usual care to improve upper limb function after stroke: the "Task-AT Home" randomised controlled trial protocol.* Frontiers in Neurology, 2023. **14**.
50. Zeiler, S.R. and J.W. Krakauer, *The interaction between training and plasticity in the poststroke brain.* Curr Opin Neurol, 2013. **26**(6): p. 609-16.

51. Nudo, R.J., et al., *Neural substrates for the effects of rehabilitative training on motor recovery after ischemic infarct.* Science, 1996. **272**(5269): p. 1791-4.
52. Takeuchi, N. and S. Izumi, *Maladaptive plasticity for motor recovery after stroke: mechanisms and approaches.* Neural Plast, 2012. **2012**: p. 359728.
53. Izawa, J., N. Higo, and Y. Murata, *Accounting for the valley of recovery during post-stroke rehabilitation training via a model-based analysis of macaque manual dexterity.* Front Rehabil Sci, 2022. **3**: p. 1042912.
54. Krakauer, J.W., et al., *Generalization of motor learning depends on the history of prior action.* PLoS Biol, 2006. **4**(10): p. e316.
55. Donchin, O., J.T. Francis, and R. Shadmehr, *Quantifying generalization from trial-by-trial behavior of adaptive systems that learn with basis functions: theory and experiments in human motor control.* J Neurosci, 2003. **23**(27): p. 9032-45.
56. Georgopoulos, A.P., et al., *Neural coding of finger and wrist movements.* J Comput Neurosci, 1999. **6**(3): p. 279-88.
57. Thoroughman, K.A. and R. Shadmehr, *Learning of action through adaptive combination of motor primitives.* Nature, 2000. **407**(6805): p. 742-7.
58. Levin, M.F. and M. Demers, *Motor learning in neurological rehabilitation.* Disabil Rehabil, 2021. **43**(24): p. 3445-3453.
59. Murata, Y., et al., *Effects of motor training on the recovery of manual dexterity after primary motor cortex lesion in macaque monkeys.* J Neurophysiol, 2008. **99**(2): p. 773-86.
60. Takei, T. and K. Seki, *Spinal interneurons facilitate coactivation of hand muscles during a precision grip task in monkeys.* J Neurosci, 2010. **30**(50): p. 17041-50.
61. Jami, L., *Golgi tendon organs in mammalian skeletal muscle: functional properties and central actions.* Physiol Rev, 1992. **72**(3): p. 623-66.
62. Schoultz, T.W. and J.E. Swett, *The fine structure of the Golgi tendon organ.* J Neurocytol, 1972. **1**(1): p. 1-26.
63. Dieterich, A.V., et al., *Spatial variation and inconsistency between estimates of onset of muscle activation from EMG and ultrasound.* Sci Rep, 2017. **7**: p. 42011.
64. Nordez, A., et al., *Electromechanical delay revisited using very high frame rate ultrasound.* J Appl Physiol (1985), 2009. **106**(6): p. 1970-5.
65. Nath, T., et al., *Using DeepLabCut for 3D markerless pose estimation across species and behaviors.* Nature Protocols, 2019. **14**(7): p. 2152-2176.
66. Mathis, A., et al., *DeepLabCut: markerless pose estimation of user-defined body parts with deep learning.* Nature Neuroscience, 2018. **21**(9): p. 1281-1289.
67. d'Avella, A., P. Saltiel, and E. Bizzi, *Combinations of muscle synergies in the construction of a natural motor behavior.* Nature Neuroscience, 2003. **6**(3): p. 300-308.

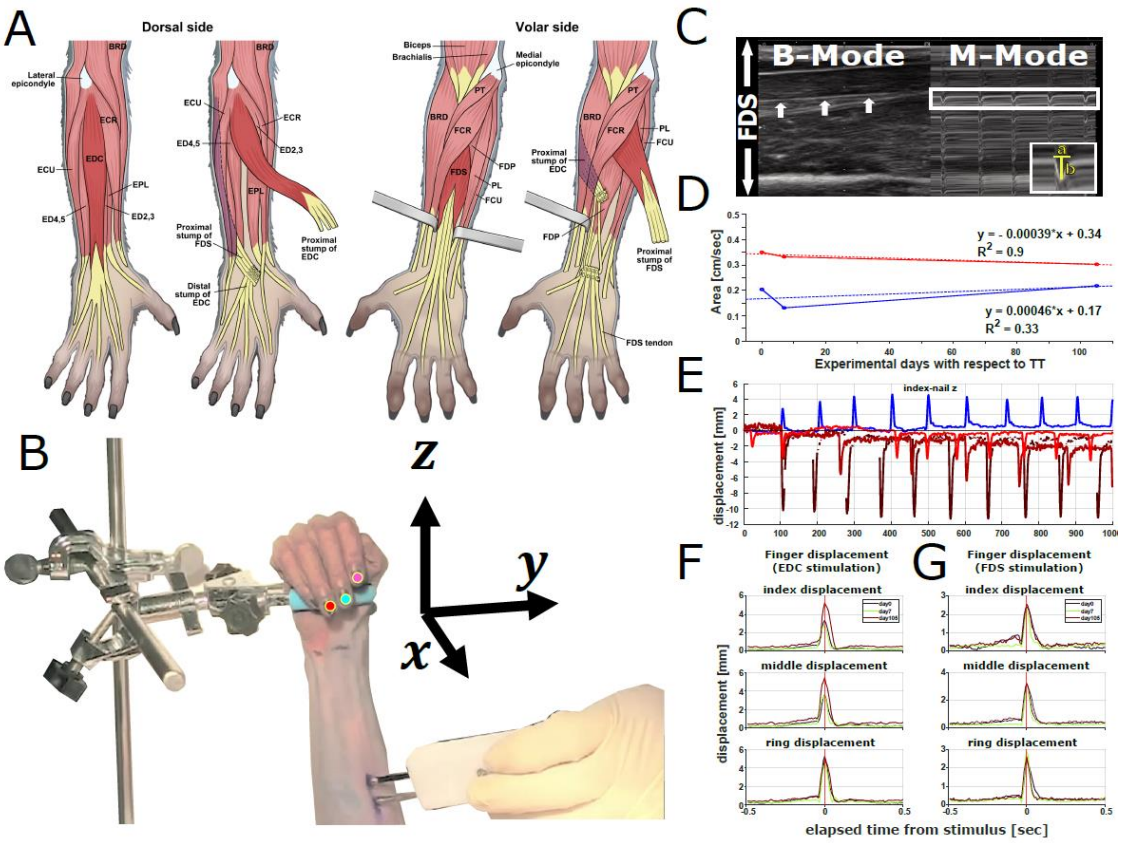

Fig.1: Surgical procedures and long term confirmation of their effectiveness to altered mechanical properties.

*(A) Muscle anatomy of the forearm of the macaque monkey. All muscles implanted with electromyography electrodes are labeled. Muscle abbreviations (Monkey A): brachioradialis (BRD), extensor carpi radialis (ECR), extensor carpi ulnaris (ECU), extensor digitorum-2,3 (ED23), extensor digitorum communis (EDC), flexor carpi radialis (FCR), flexor carpi ulnaris (FCU), flexor digitorum profundus (FDP), flexor digitorum superficialis (FDS), and palmaris longus (PL). Additionally implanted muscles in Monkey B: deltoid (DEL) and extensor digitorum-4,5 (ED45). Tendons of EDC and FDS muscles were cross-transferred. (B). Setup for ultrasound measurements and video recordings of stimulation-induced movements of EDC and FDS tendons. (C) Sonogram of FDS muscle and its intramuscular tendons. Left side (B-mode, i.e., brightness mode) shows a still image of the forearm at a given point in time. Right side (M-mode, i.e., motion mode) shows a staggered image of FDS tendon displacement induced by muscle stimulation (50 mA). White arrows demarcate the FDS tendon used for measurement. Grayscale gradations correspond to tissue densities: hyperechoic regions (white) denote denser structures like surface of bones and tendons, while hypoechoic areas (black) signify less dense tissues such as adipose tissue and musculature. The inset shows the measurement area. The displacement wave area was measured in the M-mode, and represents the strength of muscle contraction. Duration ('a' in sec) and amplitude ('b' in cm) of three waves were measured and the average calculated. Area = a*b/2(cm/sec) for days 0, 7, and 105 after tendon transfer. (D) Areas under the wave measured in the M-mode for three experimental days (0, 7, and 105 days post-TT), and*

regression lines in red and blue for FDS and EDC, respectively. $R^2 > 0.5$ for FDS. The findings suggested that muscle contractions induced by direct electrical stimulation were nearly constant. (E) Markers placed on the index, middle, and ring finger nails (B) were used to measure finger displacement in xyz-dimensions. The sum of Euclidean distances of each marker from the origin of a three-dimensional coordinate system was calculated as a scalar quantity. Movement along the z-axis was reversed post-surgery, indicating a change from finger flexion to extension due to tendon transfer (E; blue, pre-TT on surgery day; dark brown, post-TT on surgery day; light brown, 1 wk post-TT; and red, 3 wk post-TT). The scalar quantity of fingers during muscle stimulation did not change notably at days 0, 7, and 105 (F, G), suggesting there was no tendon rupture or slackening of the tendons postoperatively.

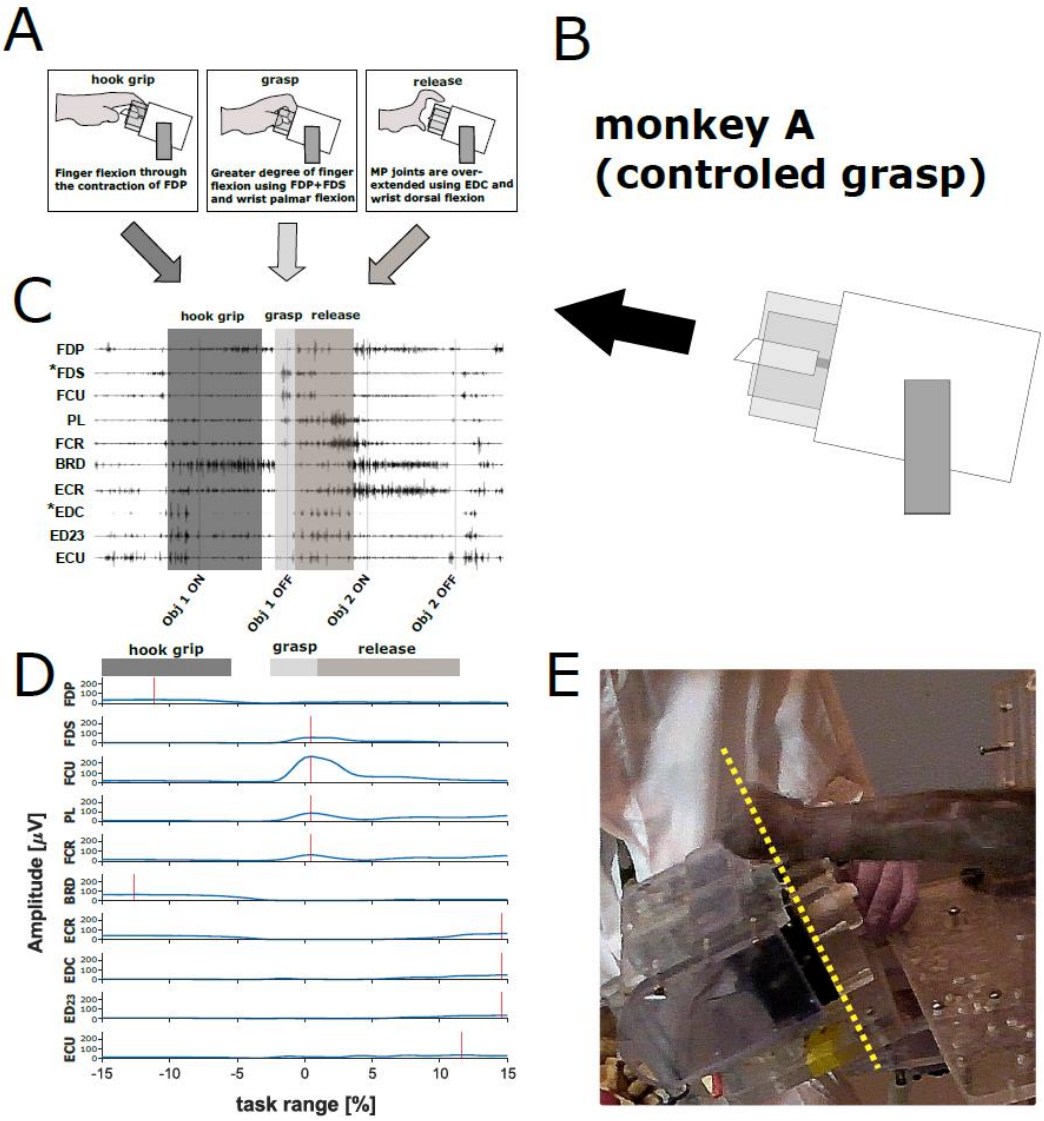

Fig. 2: Experimental set-up, task sequence, and typical electromyography.

*(A) Schematic of the behavioral sequence (hook → grasp → release). (B) Schematic of the task object using a rod, requiring Monkey A to perform a controlled grasp. (C) Typical electromyography (EMG) traces of a control session (high-pass filtered) for all recorded muscles. Gray boxes represent the task sequence. Obj 1 ON: start of hold period of object 1; Obj 1 OFF: end of hold period of object 1 (i.e., object release); Obj 2 ON: start of hold period of object 2; Obj 2 OFF: end of hold period of object 2 (i.e., object release). Muscle abbreviations: brachioradialis (BRD), extensor carpi radialis (ECR), extensor carpi ulnaris (ECU), extensor digitorum-2,3 (ED23), extensor digitorum communis (*EDC), flexor carpi radialis (FCR), flexor carpi ulnaris (FCU), flexor digitorum profundus (FDP), flexor digitorum superficialis (*FDS), and palmaris longus (PL). Tendons of muscles marked * were cross-transferred. (D) Rectified and smoothed EMG for all recorded muscles (average for one recording session; amplitude [μV] over task sequence [%]). Horizontal bars illustrate the corresponding behavioral periods and red vertical lines indicate peak amplitudes for each muscle. (E) Time the monkey spent on the left side of the yellow dotted line while moving from object 1 to object 2. This was measured and used to quantify maladaptive behavior.*

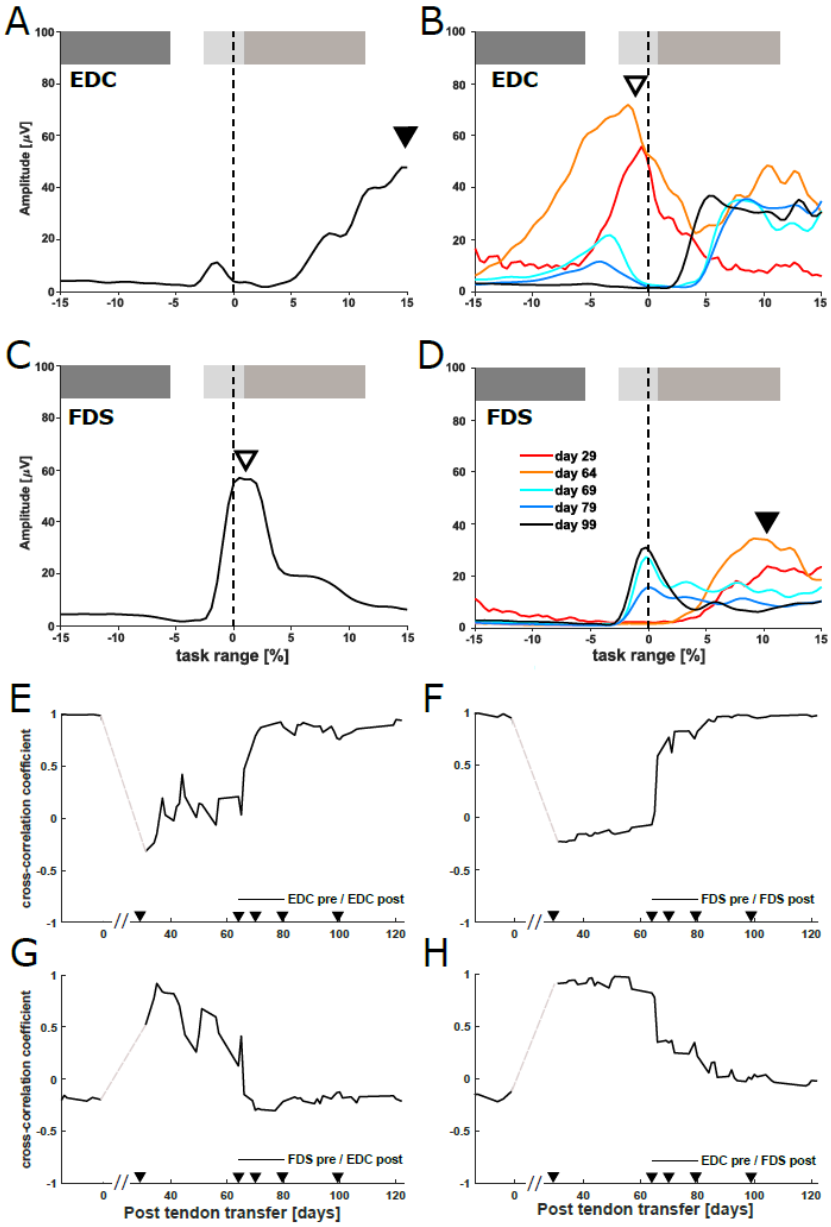

Fig. 3: Electromyography activity profiles for landmark days and cross-correlation coefficients of transferred muscles for all recording sessions.

(A, B) Electromyography (EMG) activity profiles (μV) for selected 'landmark days' pre- and post-tendon transfer (TT) of extensor digitorum communis (EDC) (A and B, respectively) in Monkey A. Profiles are aligned hold off-set (object 1) at 0% task range (vertical dashed lines). Horizontal gray bars indicate three behavioral periods: hook, grasp, and release. (C, D) As above but for flexor digitorum superficialis (FDS). Filled triangles in (A) and (D) indicate maximum EMG amplitudes for EDC before TT and FDS (during extension) immediately after TT. Open triangles indicate maximum EMG amplitudes of FDS before and EDC immediately after TT (C and B, respectively). (E-H) Cross-correlation coefficients plotted over experimental days with respect to tendon surgery. E: EDC pre/post; F: FDS pre/post; G: FDS pre/EDC post; and H: EDC pre/FDS post. Dashed lines indicate recovery periods with no recordings. Small triangles (E-H) indicate landmark days.

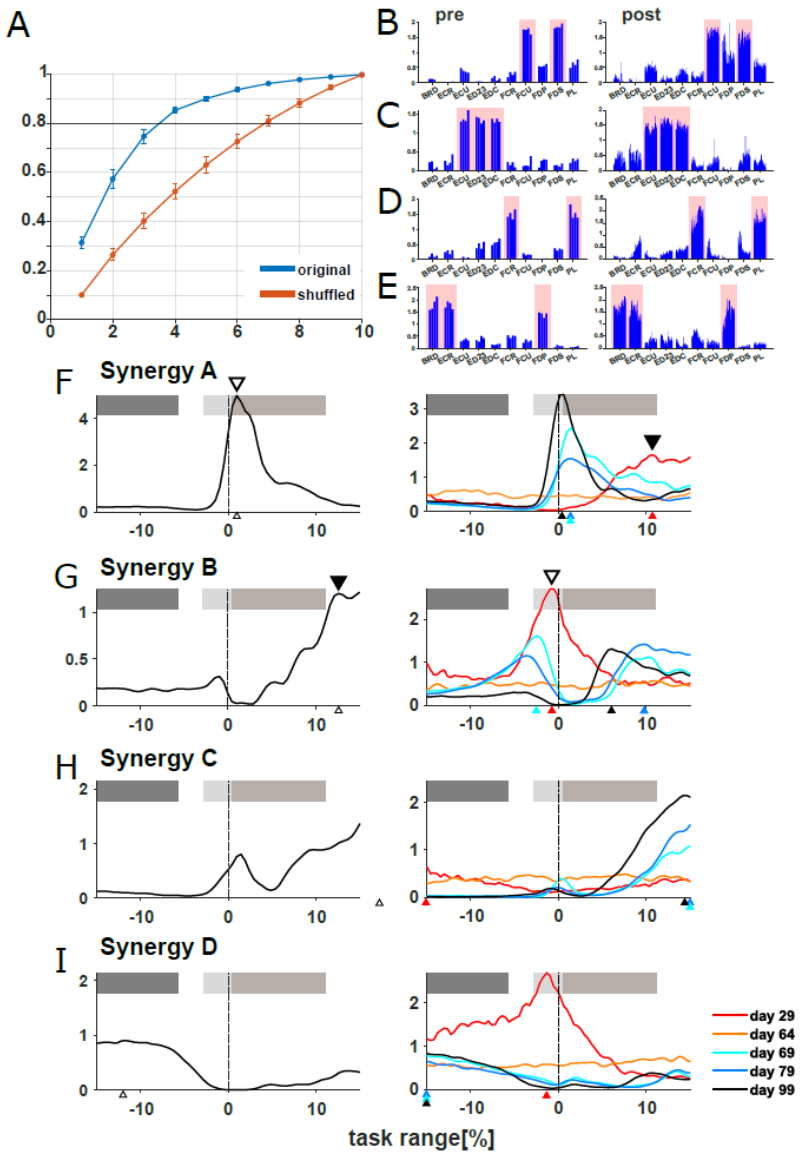

Fig. 4: Synergy weights and temporal activation coefficients.

(A) 'Variance accounted for' (VAF) for original and shuffled data of Monkey A. Four muscle synergies that accounted for > 80% of the variance were extracted from the data. (B–E) Synergy weights for each extracted muscle synergy. Each recording day was plotted individually before (left column) and after tendon transfer (TT) surgery (right column). Red boxes indicate the main contributing muscles to each corresponding synergy. (F–I) Time varying activation coefficients of muscle synergies over the task range (%) were plotted before (averaged, left column) and after TT (right column; activation coefficients for five landmark days are shown). Horizontal gray bars indicate three behavioral periods: hook, grasp, and release. Filled triangles in (F) and (G) indicate maximum amplitudes for synergy A (finger flexor synergy) immediately after TT (finger extension), and synergy B (finger extensor synergy) before TT (finger extension). Open triangles indicate maximum amplitudes for synergy A before (finger flexion) and synergy B immediately after TT (during flexion). Small triangles indicate landmark days. Profiles are aligned to hold off-set (object 1) at 0% task range.

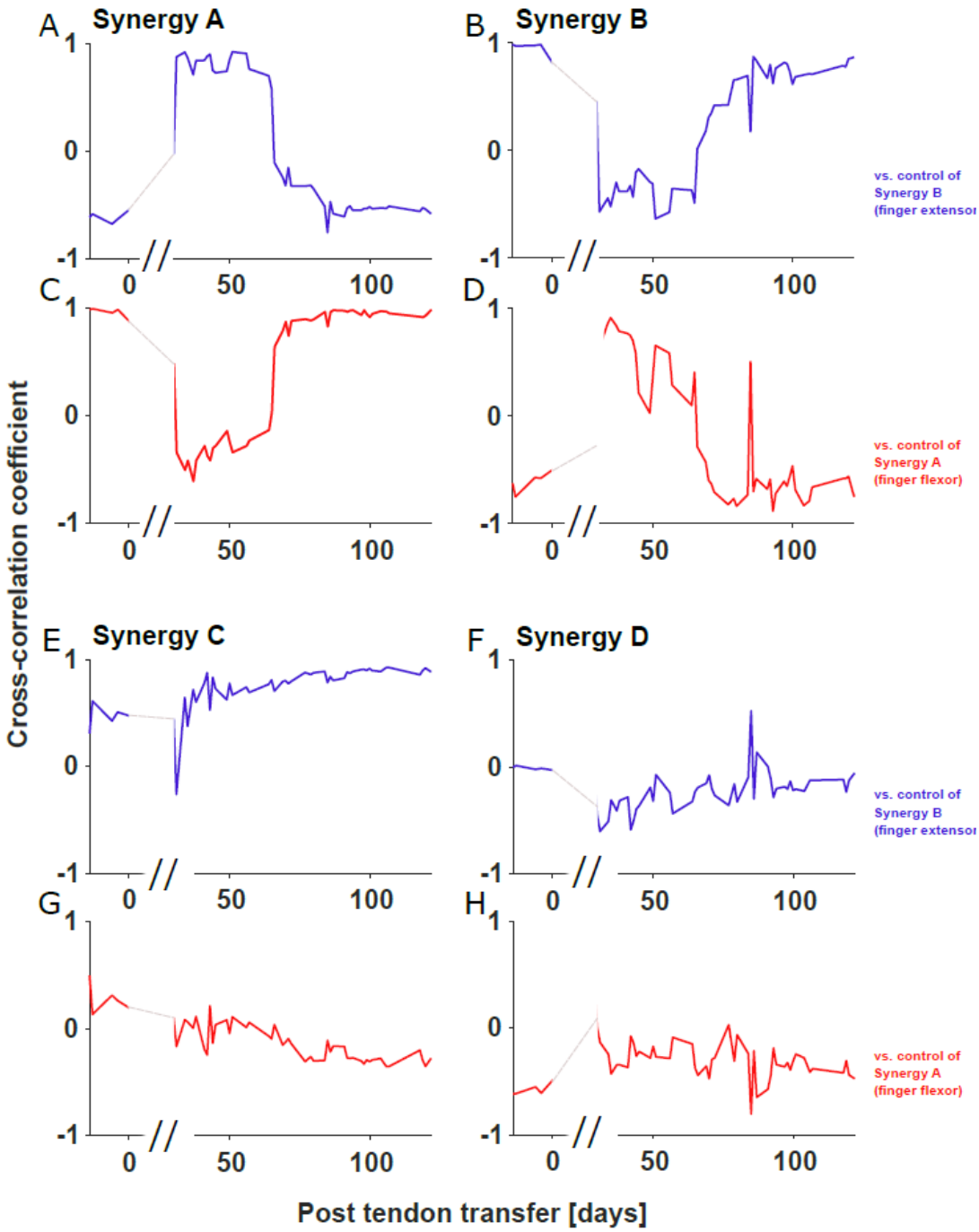

Fig. 5: Cross-correlation of muscle synergies.

Cross-correlation coefficients were plotted over experimental days with respect to tendon surgery (Monkey A). // Represents the recovery period in which no recordings were taken. Synergies were cross-correlated with either synergy A (finger flexor synergy: C, D, G, H in red) or synergy B (finger extensor synergy, A, B, E, F in blue).

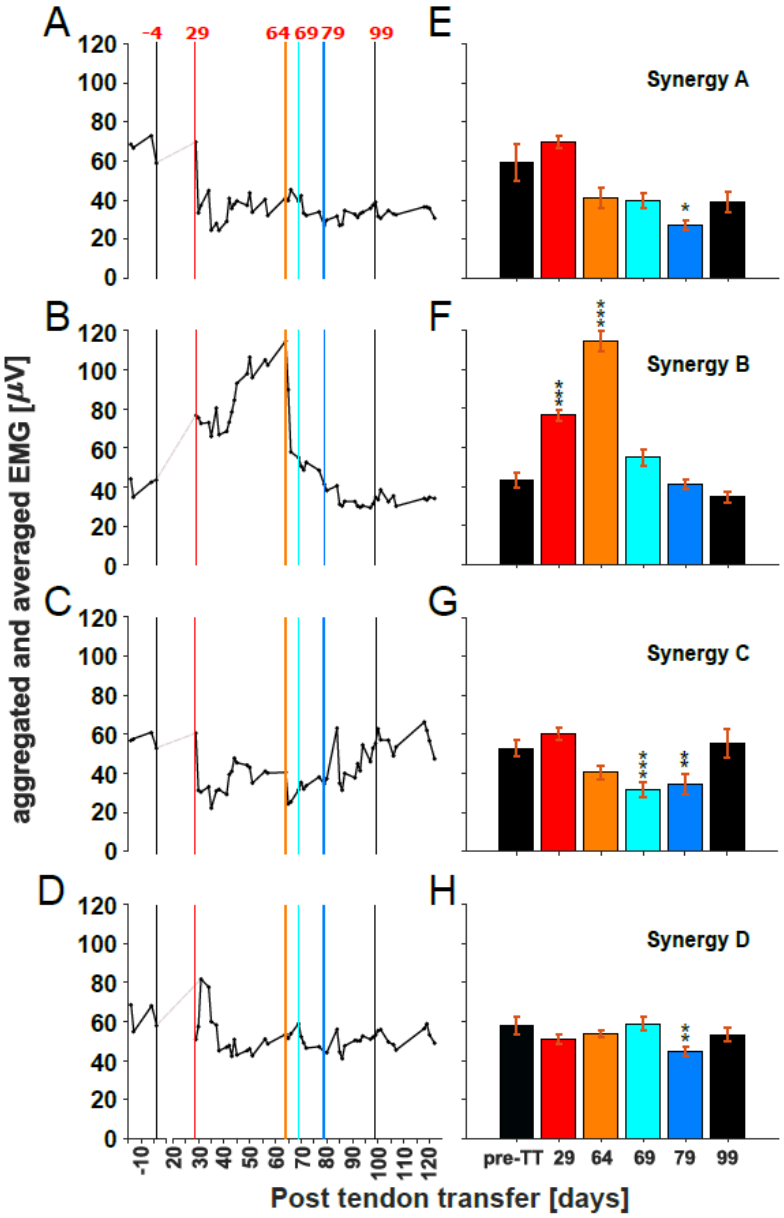

1153

1154 ***Fig. 6: Aggregated and averaged electromyography.***

1155 *Aggregated and averaged electromyography (EMG) activities of the main muscles contributing to each of four synergies for each*
1156 *recording day (Monkey A). EMG activity between −15% and +15% task range was summed for the contributing muscles and then*
1157 *averaged for each recording session. Left column: (A) synergy A, contributing muscles: flexor digitorum profundus (FDS) and*
1158 *flexor carpi ulnaris (FCU); (B) synergy B, contributing muscles: extensor digitorum communis (EDC), extensor digitorum-2,3*
1159 *(ED23), and extensor carpi ulnaris (ECU); (C) synergy C, contributing muscles: palmaris longus (PL) and flexor carpi radialis (FCR);*
1160 *and (D) synergy D, contributing muscles: flexor digitorum profundus (FDP), brachioradialis (BRD), and extensor carpi radialis*
1161 *(ECR). Vertical bars represent landmark days (red numbers at the top show actual recording days with respect to tendon transfer*
1162 *surgery). Right column: mean and standard error of the mean for landmark days. *p < 0.01, **p < 0.001, ***p < 0.0001 after*
1163 *Bonferroni correction (α = 0.01).*

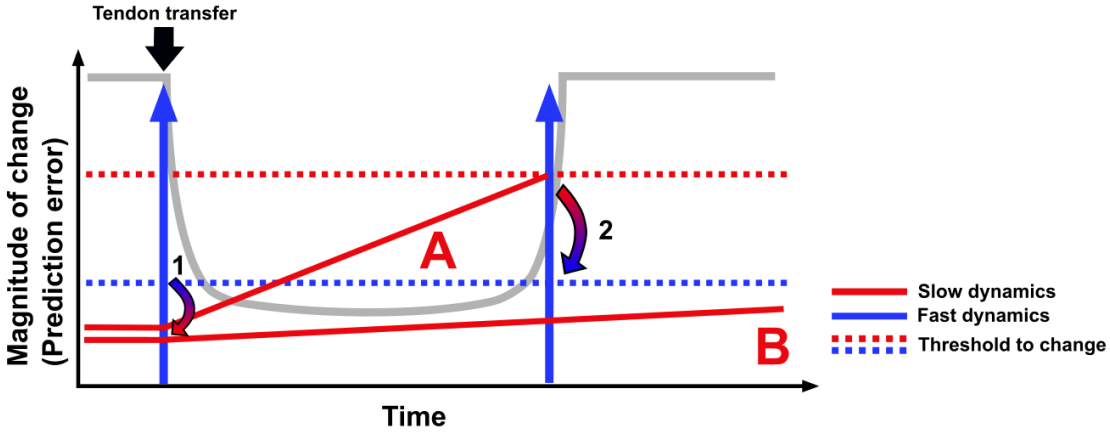

Fig. 7: Sensorimotor adaptation model following tendon transfer.

Schematic depicting the hypothesized interaction between rapid and gradual adaptation processes in the central nervous system following a significant sensory prediction error (SPE) induced by tendon transfer (TT). Our model incorporates multiple TT adaptation processes with varying timescales, encompassing both fast and slow dynamics. Tendon transfer surgery (black arrow) necessitates adjustments in finger muscle coordination, particularly a shift in the timing of activity between flexor and extensor synergies (left blue arrow). These changes exceed a critical threshold (blue dotted line), triggering slow dynamic adaptations (A and B, blue and red arrow 1). Adaptation A is faster and aims to maintain the results of the initial fast adaptation (potentially maladaptive). Meanwhile, a slower process B (background) gradually builds a new behavioral component for "good enough" task performance. This new component only becomes apparent after a second fast adaptation (second blue arrow) is triggered by process A reaching another threshold (2). At this point, the cumulative costs of the maladaptive behavior become unacceptable. The gray line represents the observed changes of cross-correlation coefficients (electromyography and temporal activation coefficients of muscle synergies).

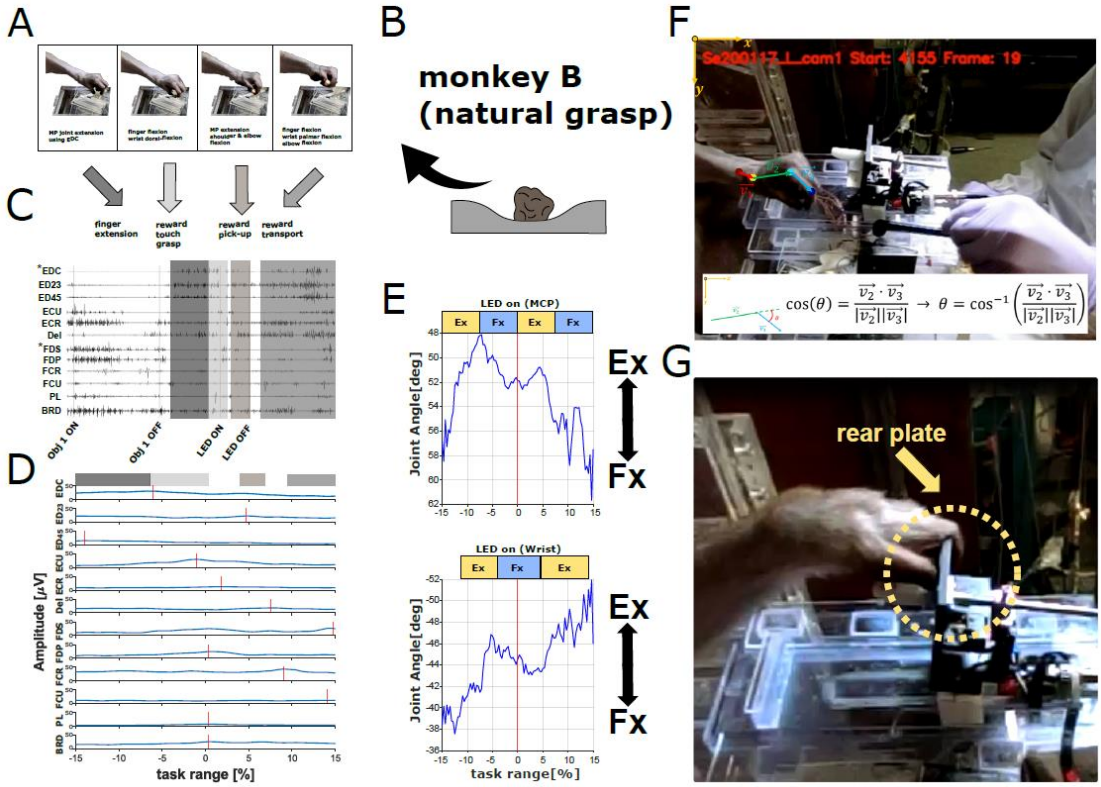

Fig. S1: Experimental setup, task sequence, and typical electromyography.

*(A) Schematic of the task sequence (picking up food). (B) Schematic of the task requiring Monkey B to pick up food from a groove, allowing for a more natural grasp. (C) Typical electromyography (EMG) traces of a control session (high-pass filtered) for all recorded muscles. Gray boxes represent the task. Obj 1 ON: start of the hold period of object 1; Obj 1 OFF: end of the hold period of object 1 (i.e., object release); LED ON: approximate start of food touch; and LED OFF: approximate time of food retrieval. Muscle abbreviations: brachioradialis (BRD), deltoid (DEL), extensor carpi radialis (ECR), extensor carpi ulnaris (ECU), extensor digitorum-2,3 (ED23), extensor digitorum-4,5 (ED45), extensor digitorum communis (*EDC), flexor carpi radialis (FCR), flexor carpi ulnaris (FCU), flexor digitorum profundus (FDP), flexor digitorum superficialis (*FDS), and palmaris longus (PL). Tendons of muscles marked * were cross-transferred. (D) Rectified and smoothed EMG for all recorded muscles (average for one recording session; amplitude [μV] over task sequence [%]). Horizontal bars represent the corresponding behavioral periods, and red vertical lines indicate peak amplitudes for each muscle. (E) Development of metacarpophalangeal (MCP) and wrist joint angles (deg) over the task range (%). Decreasing and increasing angles indicate extension or flexion of the MCP or wrist joint angle, respectively. Data are aligned to LED onset (food retrieval) and indicate consistency between behavioral observation (A), EMG (C, D), and kinematics (E). (F) Joint angle measurement using a still picture of the monkey performing the task. (G) Example of maladaptive behavior in Monkey B. Time spent in contact with or behind the object plate was measured and used to quantify the maladaptive behavior.*

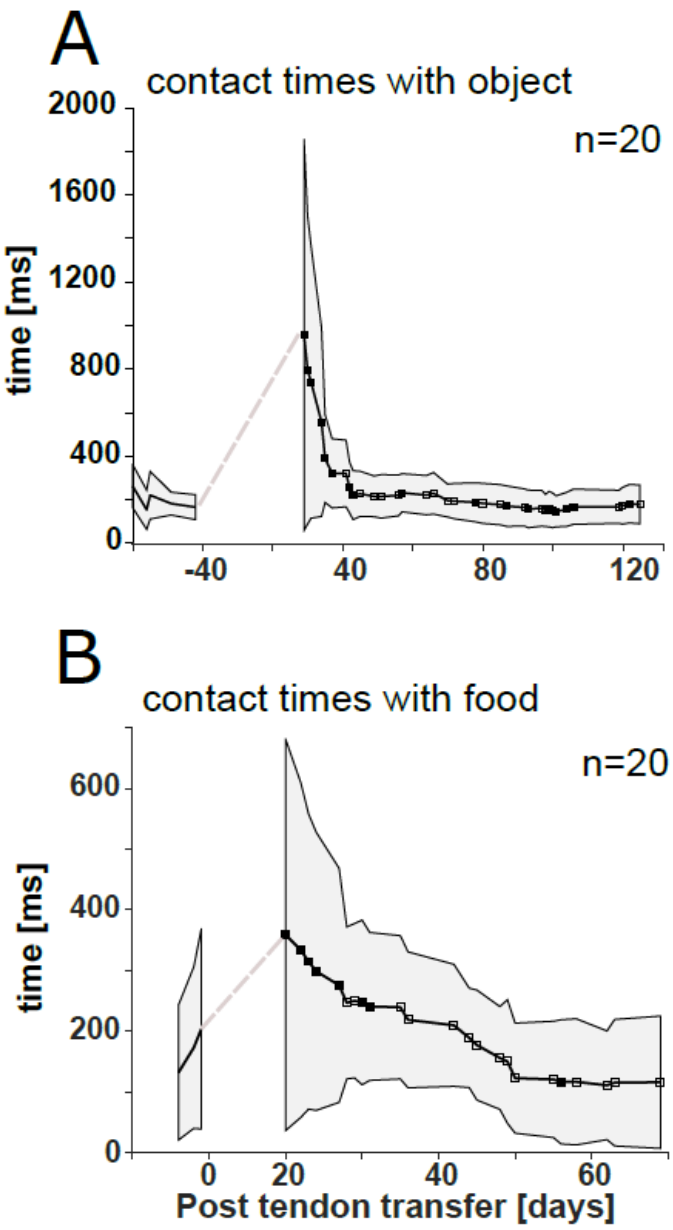

Fig. S2: Behavioral times.

(A) Contact time (ms) with the object for a controlled grasp in Monkey A. (B) Contact time with food (ms) during a natural grasp in Monkey B. Each data point represents the average of 20 observations (± SD envelope) plotted in milliseconds over days with respect to tendon transfer (TT) (day 0). Open squares: n.s.; and filled squares: $p < 0.05$, two-sample t-test.

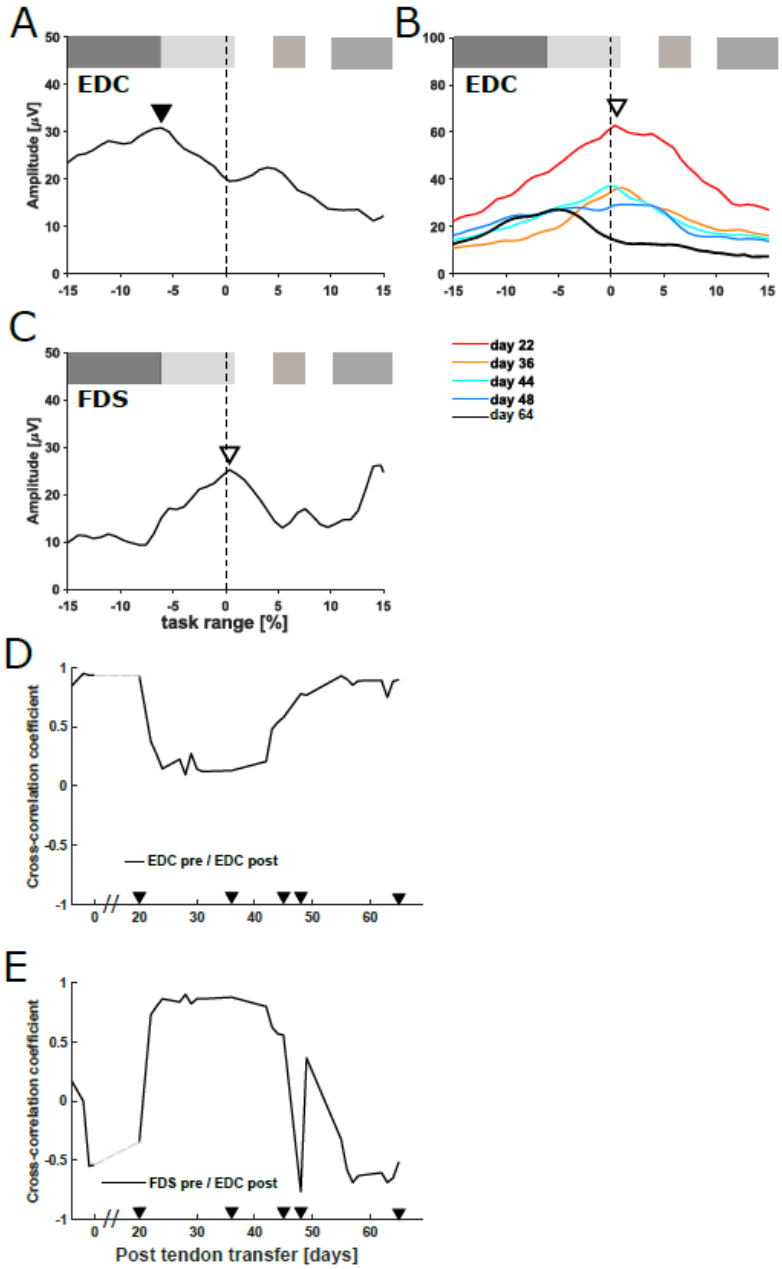

Fig. S3: Electromyography activity profiles of landmark days and cross-correlation coefficients of transferred muscles for all recording sessions.

(A, B) Electromyography (EMG) activity profiles (μV) of selected 'landmark days' for pre- and post-tendon transfer (TT) days of extensor digitorum communis (EDC) (A and B, respectively) of Monkey B. Profiles are aligned to LED onset (food touch) at 0% task range (dashed lines). Horizontal gray bars indicate four behavioral periods: finger extension, food touch, food pick-up, and food transport. (C) As above but for flexor digitorum superficialis (FDS). (D, E) Cross-correlation coefficients plotted over experimental days with respect to tendon surgery. (D) EDC pre/post; and E: FDS pre/EDC post. The filled triangle in (A) indicates the maximum EMG amplitude for EDC before TT. Open triangles indicate the maximum EMG amplitude of FDS before and EDC immediately after TT (C and B, respectively). Small triangles (D, E) indicate landmark days.

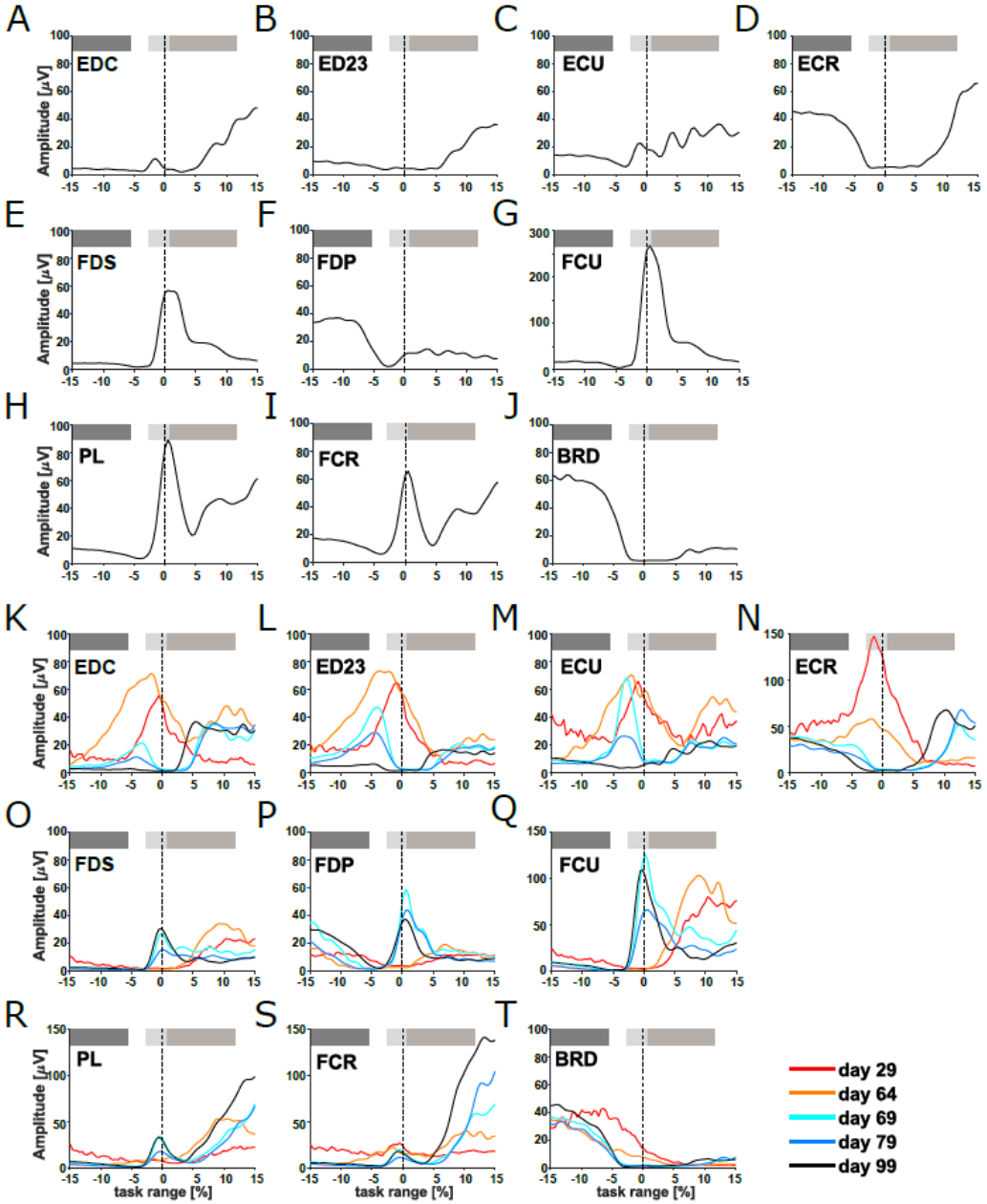

Fig. S4: Electromyography activity profiles of landmark days (Monkey A).

Electromyography activity profiles (µV) of selected 'landmark days' for all recorded muscles (pre- and post-tendon transfer [TT]; A-J and K-T, respectively). Profiles are aligned to hold off-set (object 1) at 0% task range (dashed lines). Horizontal gray bars indicate three behavioral periods: hook, grasp, and release.

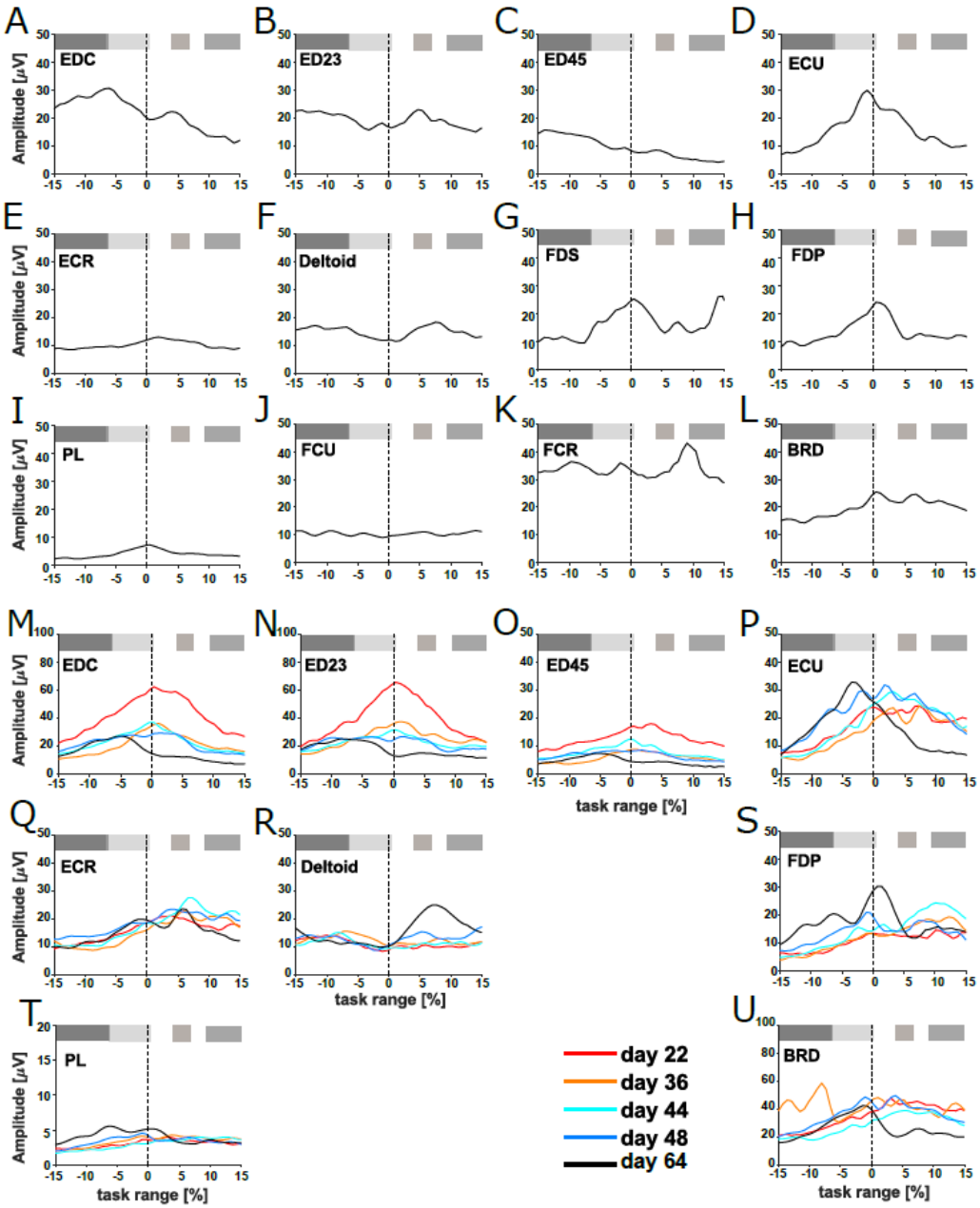

1218

1219 ***Fig. S5: Electromyography activity profiles of landmark days (Monkey B).***

1220 *Electromyography activity profiles (μV) of selected 'landmark days' for all recorded muscles (pre- and post-tendon transfer*

1221 *[TT]; A-L and M-U, respectively). Profiles are aligned to LED onset (food touch) at 0% task range (dashed lines). Horizontal gray*

1222 *bars indicate four behavioral periods: finger extension, food touch, food pick-up, and food transport.*

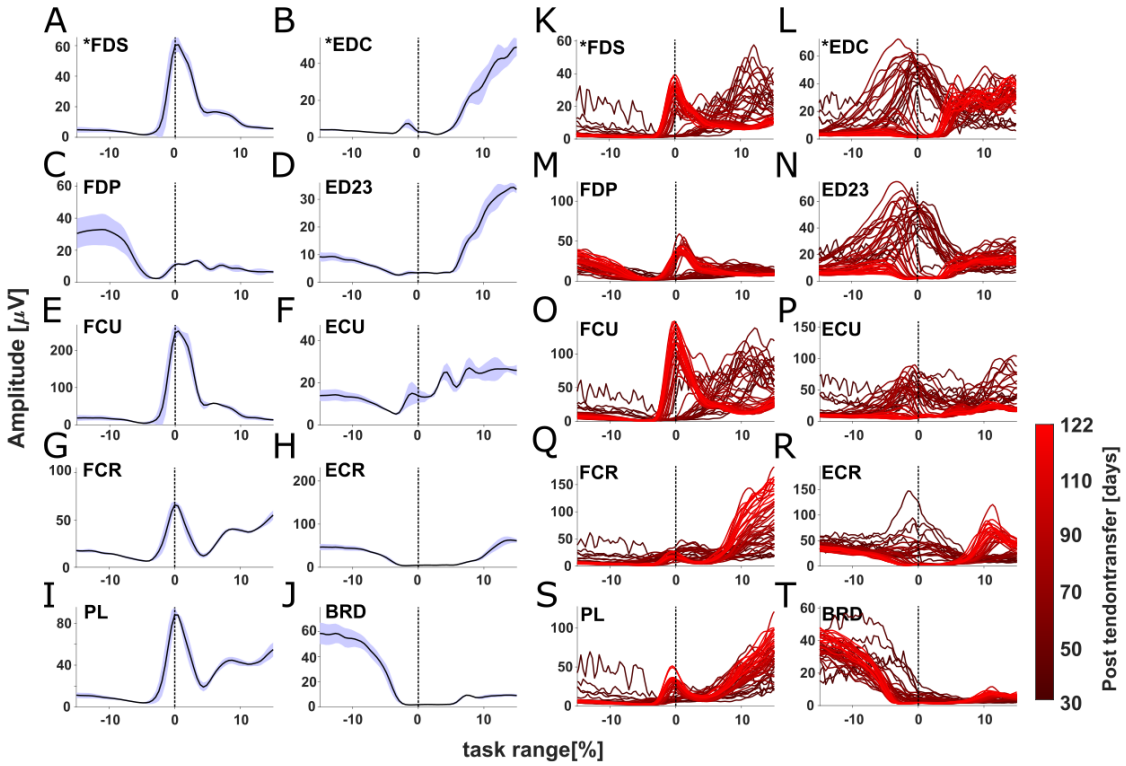

Fig. S6: Electromyography activity profiles for all sessions over time (Monkey A).

*Electromyography (EMG) activity profiles before tendon transfer (TT) (average of four pre-TT sessions ± SD in blue [A-J] and for each day post-TT [K-T]) for all recorded muscles aligned to hold off-set (object 1) at 0% task range. Y-axis: EMG amplitude (μV). Darker colors indicate early and lighter colors later recording days post-TT, starting with day 29 (see color bar). Muscle tendons marked * were cross-transferred.*

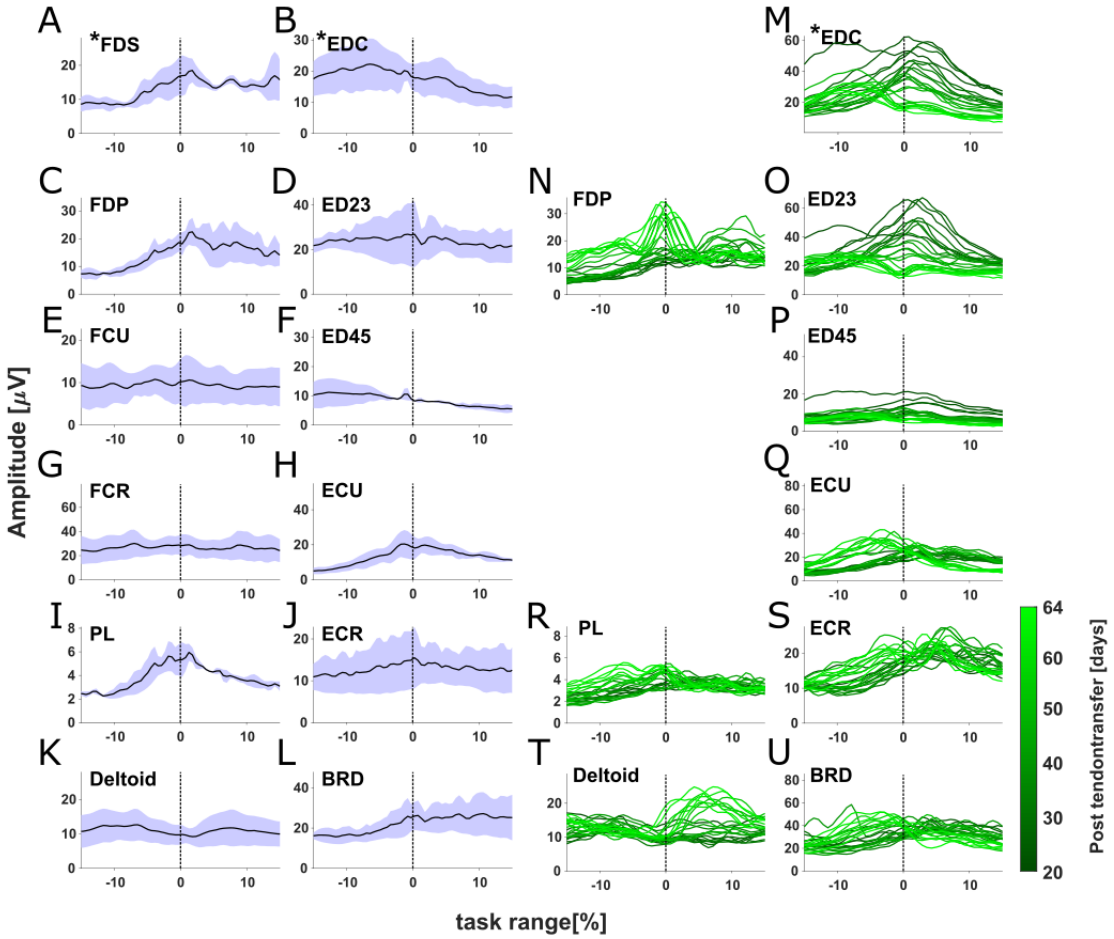

Fig. S7: Electromyography activity profiles for all sessions over time (Monkey B).

*Electromyography (EMG) activity profiles before tendon transfer (TT) (average of three pre-TT sessions ± SD in blue [A-L] and for each day post-TT [M-U]) for all recorded muscles aligned to photo LED onset (food touch) at 0% task range. Y-axis: EMG amplitude (μV). Darker colors indicate early and lighter colors later recording days post-TT, starting with day 20 (see color bar). Muscle tendons marked * were cross-transferred.*

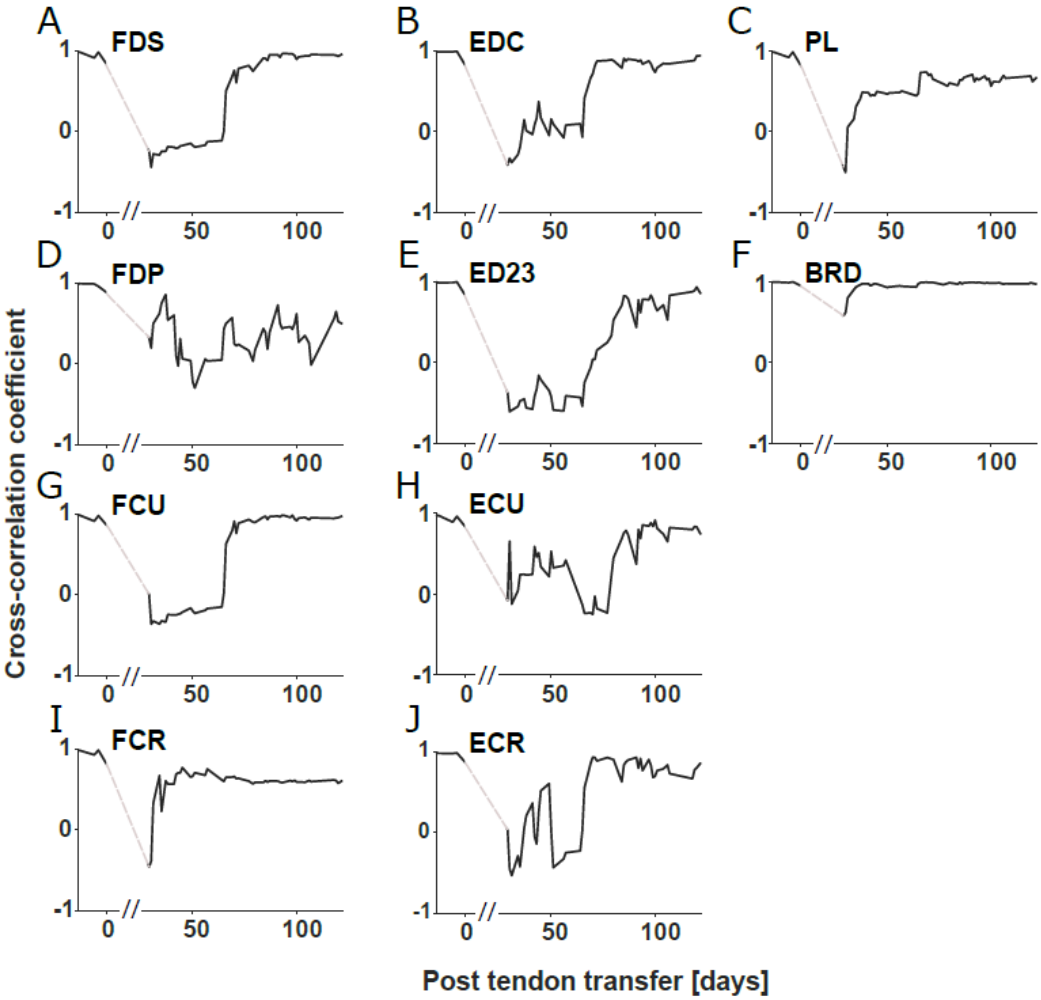

Fig. S8: Cross-correlation analysis for Monkey A.

Cross-correlation coefficients plotted over experimental days with respect to tendon surgery in Monkey A. Each muscle was cross-correlated with its own control data recorded prior to tendon transfer surgery.

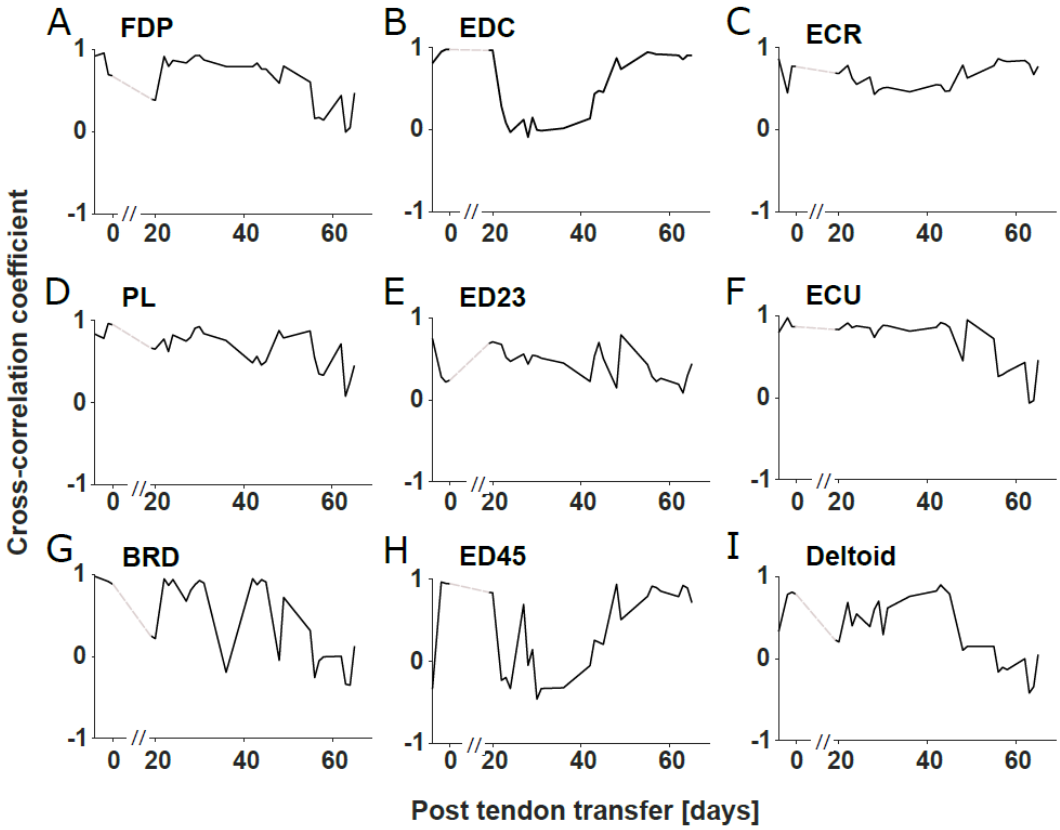

Fig. S9: Cross-correlation analysis for Monkey B.

Cross-correlation coefficients plotted over experimental days with respect to tendon surgery in Monkey B. Each muscle was cross-correlated with its own control data recorded prior to tendon transfer surgery.

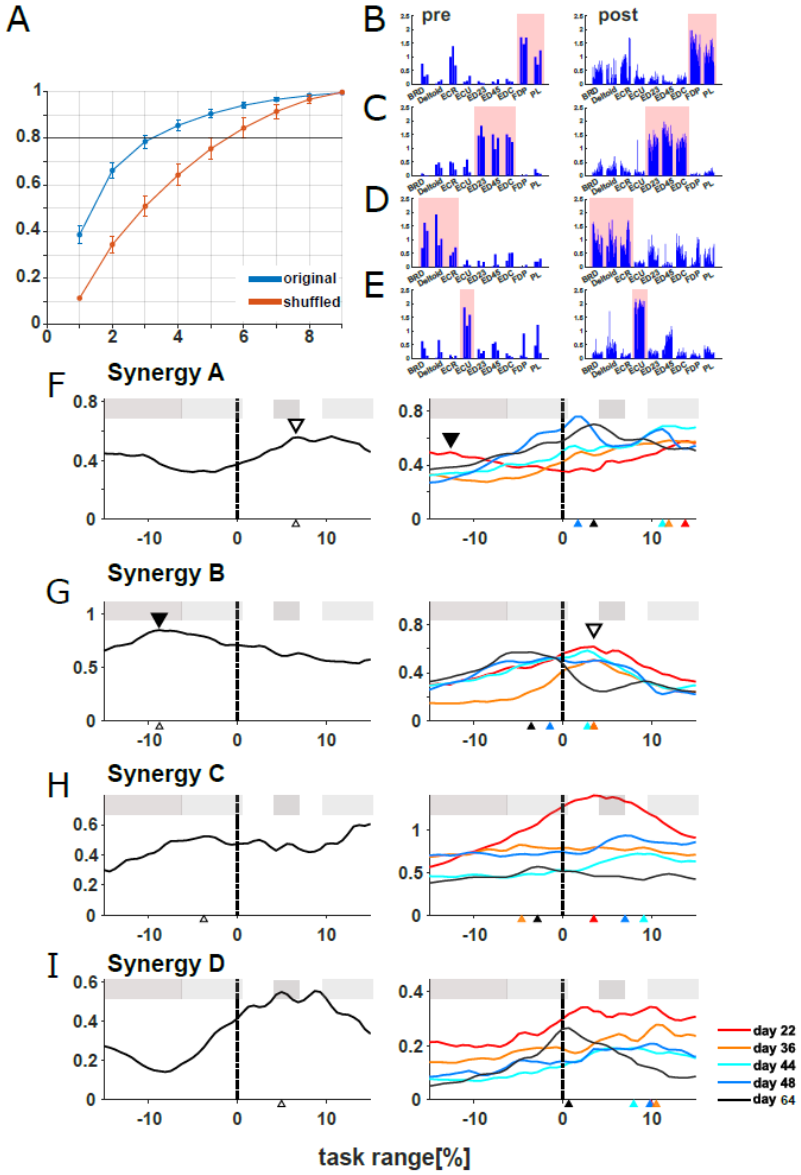

Fig. S10: Synergy weights and temporal activation coefficients.

(A) 'Variance accounted for' (VAF) for original and shuffled data (Monkey B). Four muscle synergies that accounted for > 80% of variance were extracted from the data. (B–E) Synergy weights for each extracted muscle synergy. Each recording day was plotted individually before (left column) and after tendon transfer (TT) surgery (right column). Red boxes indicate the main contributing muscles to each corresponding synergy. (F–I) Time varying activation coefficients of muscle synergies over task range (%) were plotted before (averaged, left column) and after TT (right column; activation coefficients for five landmark days are shown). Horizontal gray bars indicate four behavioral periods: finger extension, food touch, food pick-up, and food transport. Filled triangles in (F) and (G) indicate maximum amplitudes for synergy A (finger flexor synergy) immediately after TT (finger extension), and synergy B (finger extensor synergy) before TT (finger extension). Open triangles indicate maximum amplitudes for synergy A before (finger flexion) and synergy B immediately after TT (during flexion). Small triangles indicate landmark days. Profiles are aligned to LED onset (food touch) at 0% task range.

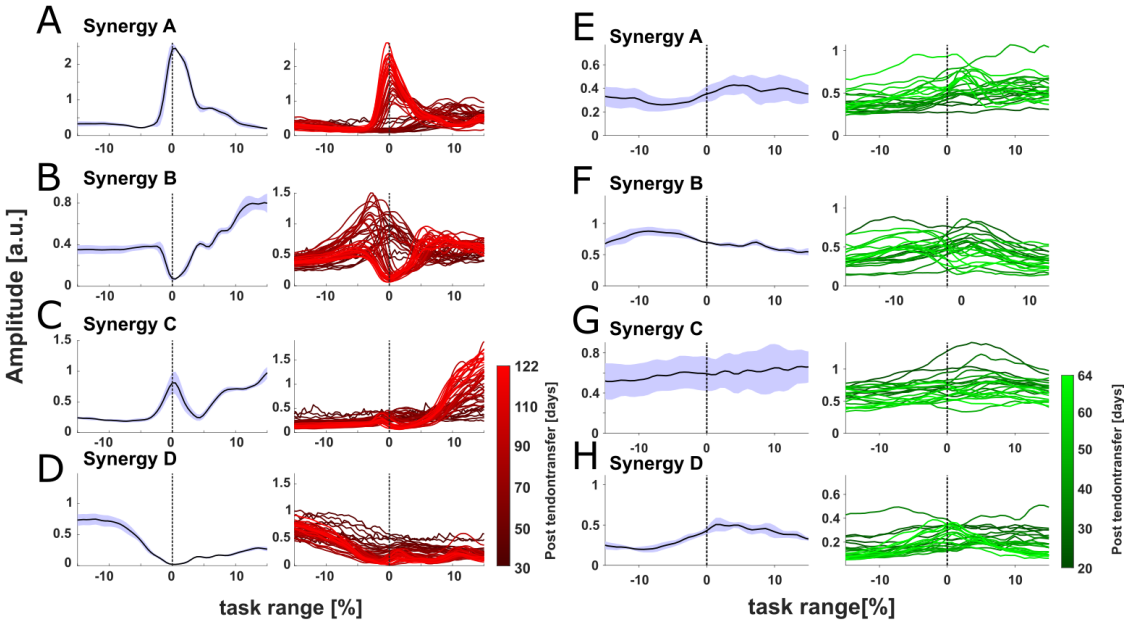

Fig. S11: Time varying activation coefficients for muscle synergies.

(A–D) Temporal synergies of Monkey A. The left column shows mean activation coefficients of control data for all four synergies (synergy A–D) with the corresponding standard deviation (blue envelope) aligned to hold off-set (object 1) at 0% task range (dashed lines). The right column shows temporal activation coefficients for each recording day post-tendon transfer surgery (red lines; darker and lighter colors represent early and late recording days, respectively). (E–H) As for Monkey B. Profiles are aligned to LED onset (food touch) at 0% task range.

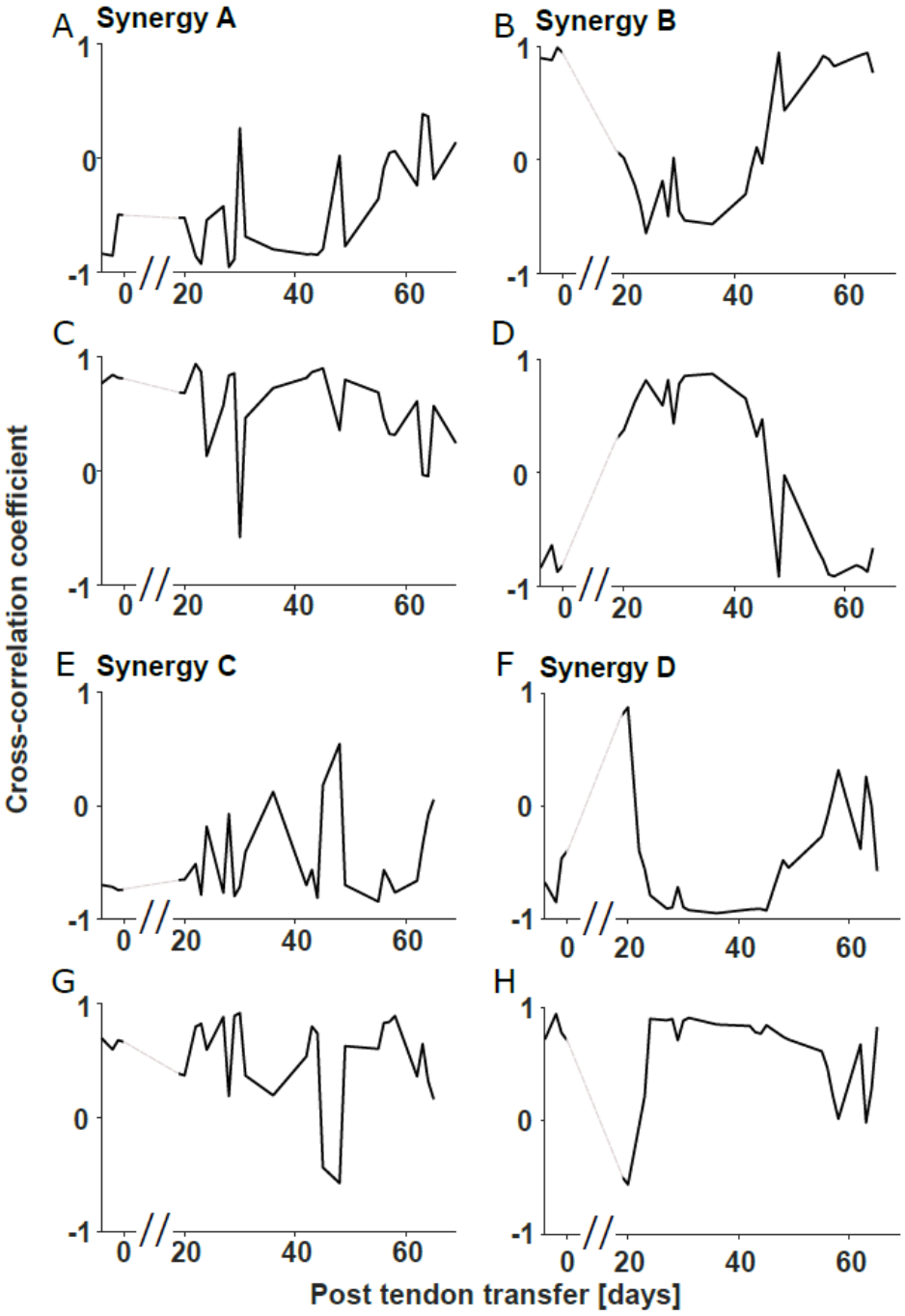

Fig. S12: Cross-correlation of muscle synergies.

Cross-correlation coefficients plotted over experimental days with respect to tendon surgery (Monkey B). // Represents the recovery period in which no recordings were taken. Synergies were cross-correlated with either synergy A (flexor synergy, C, D, G, H) or synergy B (extensor synergy, A, B, E, F).

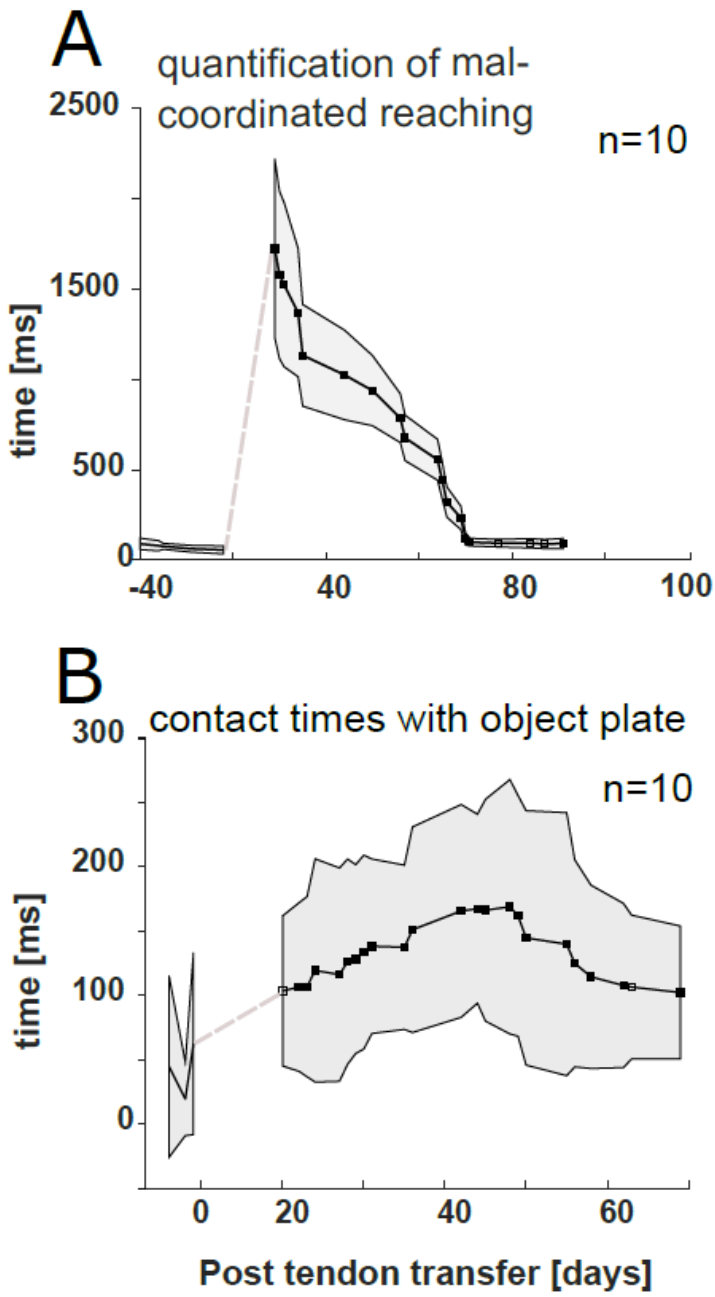

Fig. S13: Behavioral analysis of maladaptation.

(A) Quantification of malcoordinated behavior in Monkey A. Duration (ms) spent on the left side of the yellow dotted line while moving from object 1 to object 2 (see Fig. 2E). (B) Contact time (ms) with the object plate for Monkey B was used to quantify malcoordinated reaching behavior. Each data point represents the average of 10 observations (± SD envelope) plotted over days with respect to tendon transfer (TT) (day 0). Open circles: n.s.; and filled circles: $p < 0.05$, two-sample t-test.

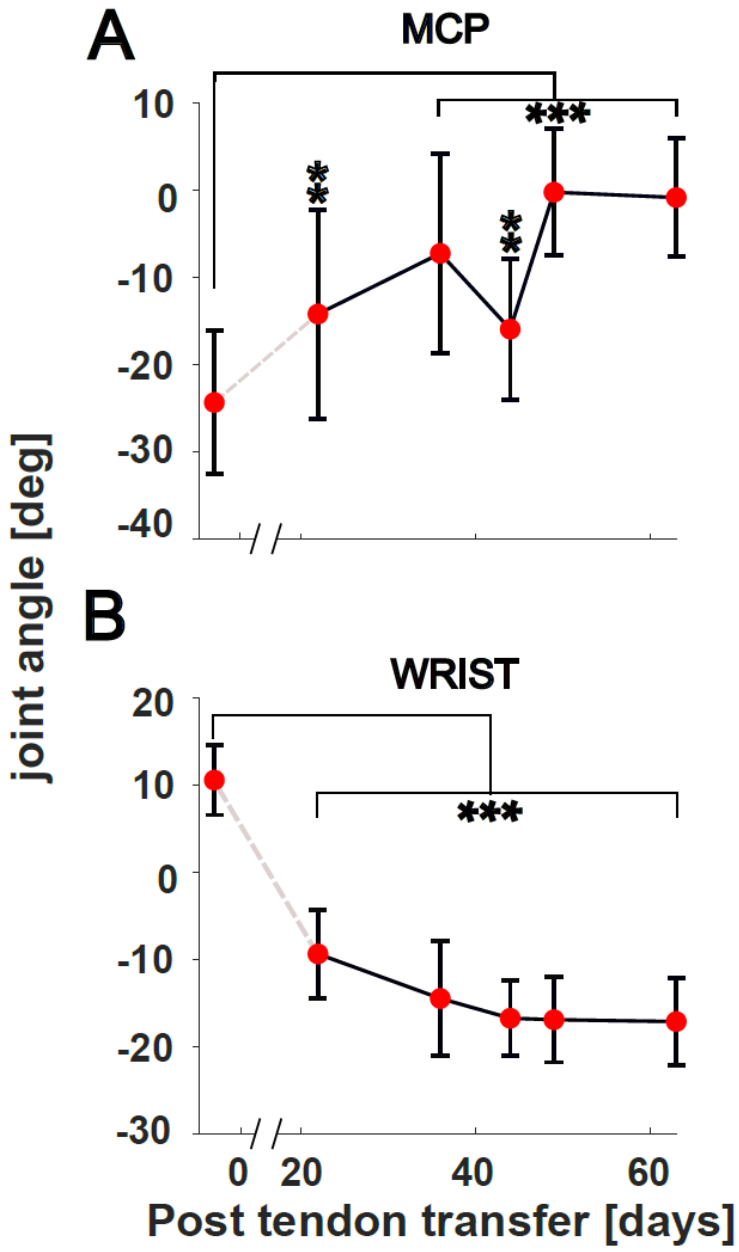

Fig. S14: Changes in joint angles following tendon transfer.

Changes in the angle of two key joints in Monkey B before and after tendon transfer (TT) surgery (mean of 20 trials ± SD for each landmark day, taken 83 ms before food touch). The angle at the metacarpophalangeal (MCP) joint (A), responsible for finger extension, steadily increased following surgery (indicating increased finger extension). Concurrently, the wrist joint angle (B) decreased, indicating wrist flexion. Statistical analysis confirmed these changes were significant ($p < 0.01$, ANOVA; $\alpha = 0.01$). This coordinated movement pattern suggests a potential compensatory strategy employed by the monkey to achieve finger extension during grasping tasks. // Represents the recovery period in which no recordings were taken.

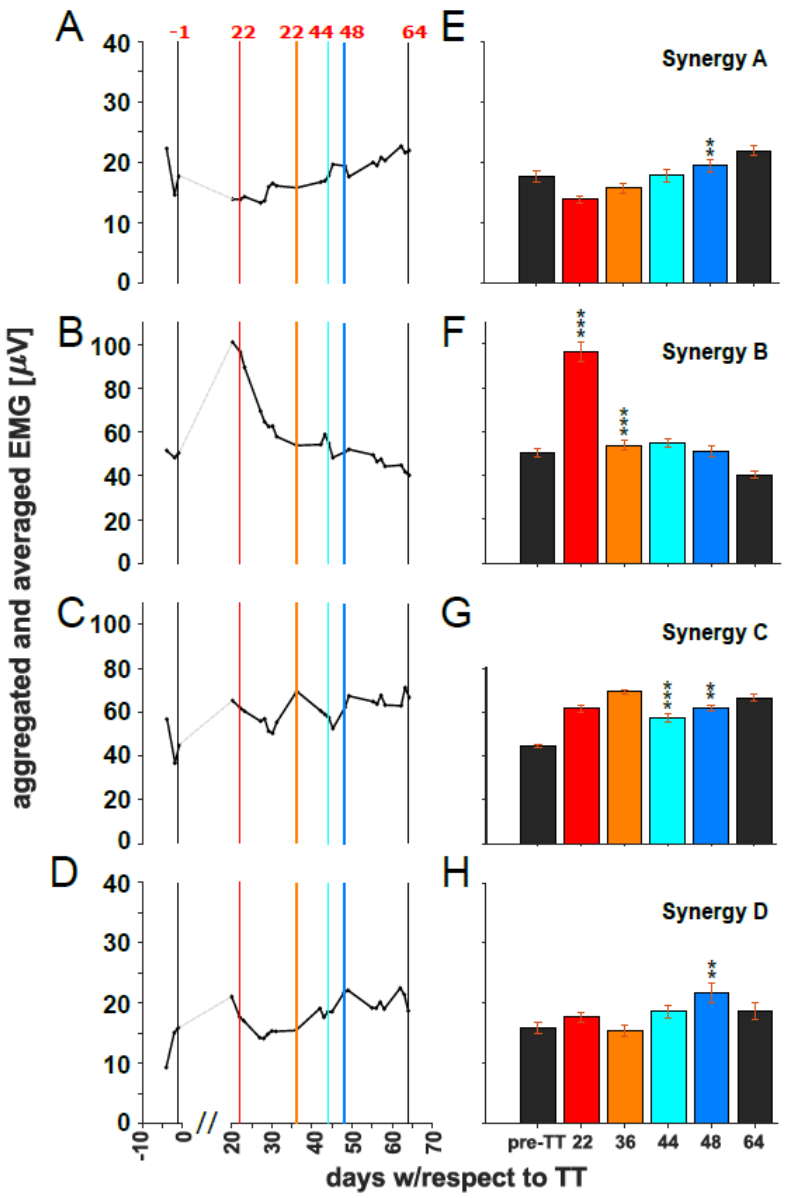

Fig. S15: Aggregated and averaged electromyography in Monkey B.

*Aggregated and averaged electromyography (EMG) activities of the main muscles contributing to each of the four synergies for each recording day. EMG activity between −15% and +15% task range were summed for the contributing muscles and then averaged for each recording session. Left column: (A) synergy A, contributing muscles: flexor digitorum profundus (FDP) and palmaris longus (PL); (B) synergy B, contributing muscles: extensor digitorum communis (EDC), extensor digitorum−2,3 (ED23), and extensor digitorum−4,5 (ED45); (C) synergy C, contributing muscles: extensor carpi radialis (ECR), brachioradialis (BRD), and deltoid (DEL); and (D) synergy D, contributing muscles: extensor carpi ulnaris (ECU). // Represents the recovery period in which no recordings were taken. Vertical bars represent landmark days (red numbers at the top show actual recording days with respect to tendon transfer [TT] surgery). Right column: Mean and standard error of the mean for landmark days. * $p < 0.01$, ** $p < 0.001$, *** $p < 0.0001$ after Bonferroni correction ($\alpha = 0.01$).*